



**AFRL-AFOSR-VA-TR-2019-0330**

---

On-chip Quantum Memories at Telecom Wavelengths Based on  
Er<sup>3+</sup>:YSO Nano-Photonic Resonators

**Andrei Faraon**  
**CALIFORNIA INSTITUTE OF TECHNOLOGY**  
**1200 E. CALIFORNIA BLDV**  
**PASADENA, CA 91125**

---

**11/08/2019**  
**Final Report**

**DISTRIBUTION A: Distribution approved for public release.**

Air Force Research Laboratory  
AF Office Of Scientific Research (AFOSR)/RTB1

DISTRIBUTION A: Distribution approved for public release

Arlington, Virginia 22203  
Air Force Materiel Command

<b>REPORT DOCUMENTATION PAGE</b>				<i>Form Approved</i> OMB No. 0704-0188	
<p>The public reporting burden for this collection of information is estimated to average 1 hour per response, including the time for reviewing instructions, searching existing data sources, gathering and maintaining the data needed, and completing and reviewing the collection of information. Send comments regarding this burden estimate or any other aspect of this collection of information, including suggestions for reducing the burden, to Department of Defense, Executive Services, Directorate (0704-0188). Respondents should be aware that notwithstanding any other provision of law, no person shall be subject to any penalty for failing to comply with a collection of information if it does not display a currently valid OMB control number.</p> <p><b>PLEASE DO NOT RETURN YOUR FORM TO THE ABOVE ORGANIZATION.</b></p>					
<b>1. REPORT DATE (DD-MM-YYYY)</b> 08-11-2019		<b>2. REPORT TYPE</b> Final Performance		<b>3. DATES COVERED (From - To)</b> 15 Aug 2015 to 14 Aug 2018	
<b>4. TITLE AND SUBTITLE</b> On-chip Quantum Memories at Telecom Wavelengths Based on Er <sup>3+</sup> :YSO Nano-Photonic Resonators				<b>5a. CONTRACT NUMBER</b>	
				<b>5b. GRANT NUMBER</b> FA9550-15-1-0252	
				<b>5c. PROGRAM ELEMENT NUMBER</b> 61102F	
<b>6. AUTHOR(S)</b> Andrei Faraon				<b>5d. PROJECT NUMBER</b>	
				<b>5e. TASK NUMBER</b>	
				<b>5f. WORK UNIT NUMBER</b>	
<b>7. PERFORMING ORGANIZATION NAME(S) AND ADDRESS(ES)</b> CALIFORNIA INSTITUTE OF TECHNOLOGY 1200 E. CALIFORNIA BLDV PASADENA, CA 91125 US				<b>8. PERFORMING ORGANIZATION REPORT NUMBER</b>	
<b>9. SPONSORING/MONITORING AGENCY NAME(S) AND ADDRESS(ES)</b> AF Office of Scientific Research 875 N. Randolph St. Room 3112 Arlington, VA 22203				<b>10. SPONSOR/MONITOR'S ACRONYM(S)</b> AFRL/AFOSR RTB1	
				<b>11. SPONSOR/MONITOR'S REPORT NUMBER(S)</b> AFRL-AFOSR-VA-TR-2019-0330	
<b>12. DISTRIBUTION/AVAILABILITY STATEMENT</b> A DISTRIBUTION UNLIMITED: PB Public Release					
<b>13. SUPPLEMENTARY NOTES</b>					
<b>14. ABSTRACT</b> Quantum memories for light are important components for future long distance quantum networks. We demonstrated on-chip quantum storage of telecommunications band light at the single photon level in an ensemble of erbium-167 ions in an yttrium orthosilicate photonic crystal nanobeam resonator. Storage times of up to 10 microseconds are demonstrated using an all-optical atomic frequency comb protocol at dilution refrigerator temperatures under a magnetic field of 380 mT. We show this quantum storage platform to have high bandwidth, high fidelity, and multimode capacity, and we outline a path towards an efficient erbium-167 quantum memory for light.					
<b>15. SUBJECT TERMS</b> quantum memories, photonic resonators, Purcell effect, quantum optics, rare earth, on-chip nano-scale optical quantum memories					
<b>16. SECURITY CLASSIFICATION OF:</b>			<b>17. LIMITATION OF ABSTRACT</b>  UU	<b>18. NUMBER OF PAGES</b>	<b>19a. NAME OF RESPONSIBLE PERSON</b> POMRENKE, GERNOT
<b>a. REPORT</b>  Unclassified	<b>b. ABSTRACT</b>  Unclassified	<b>c. THIS PAGE</b>  Unclassified			<b>19b. TELEPHONE NUMBER (Include area code)</b> 703-696-8426

Final Report: AFOSR-YIP

Grant Number: FA9550-15-1-0252 Period Covered: 08/15/2015-8/14/2018

PI: Andrei Faraon

California Institute of Technology, Pasadena, CA, 91125 [Faraon@caltech.edu](mailto:Faraon@caltech.edu)

Proposal title: On-chip Quantum Memories at Telecom Wavelengths Based on Er<sup>3+</sup>:YSO Nano-Photonic Resonators

### Summary:

The objective of this proposal is to develop on-chip nano-scale optical quantum memories operating at telecom wavelength. These are key elements for implementing optical fiber networks for quantum key distribution. To date, there are no demonstrations of efficient quantum memories for coupling to fibers. Atomic ensembles don't operate in the telecom band, and solid-state memories based on macroscopic erbium-doped crystals and fibers suffer from poor efficiency because of imperfect optical pumping.

To surpass this limitation, we proposed to develop optical memories based on photonic nano-resonators fabricated in erbium doped yttrium orthosilicate (Er<sup>3+</sup>:YSO), a technology that our lab has successfully pioneered. YSO is the leading material choice for solid-state quantum memories. 69% efficient optical memory and storage of entangled photons were demonstrated with Pr<sup>3+</sup>:YSO and Nd<sup>3+</sup>:YSO respectively. By coupling to nano-resonators, the spontaneous emission rate from Er<sup>3+</sup> will be strongly enhanced via the Purcell effect, thus leading to improved optical pumping and increased memory efficiency. Coupling with high cooperativity allows for large optical depth in ultra-compact nano-resonators and integration into photonic networks.

### **The project has the following aims/objectives, all of which have been accomplished.**

1. Fabricate high-quality nanophotonic resonators coupled to Er<sup>3+</sup> in yttrium orthosilicate (YSO) for operation at 1536nm. Toward this goal we developed photonic crystal nano-resonators fabricated directly in YSO via focused ion beam milling. We demonstrated coupling of the Er to the resonator. This work was published in Miyazono et al, Applied Physics Letters 108, 011111 (2016). We also demonstrated silicon resonators coupled evanescently to erbium ions in YSO. This result was published in Miyazono et al, Optics Express Vol. 25, Issue 3, pp. 2863-2871 (2017)
2. Study of the quantum optical properties of Er<sup>3+</sup> coupled to the nano-cavity. Our measurements show that the properties of the Er ions in the cavity are the same as the properties of the ions in bulk material and thus are suitable for on-chip quantum memories.
3. Demonstrate on-chip optical storage and retrieval of telecom wavelength photons from an Er<sup>3+</sup> ensemble coupled to a nano-cavity. We demonstrated proof of concept atomic frequency comb quantum memories in our devices.

Besides accomplishing the aims, people supported by this grant also contributed to other projects and publications. These include our recent *Science* paper where we demonstrated nano-photonic quantum memories in neodymium doped materials. Another project resulted in a paper in *Nature* where we demonstrated deterministic placement of quantum emitters using DNA origami.

### Publications:

1. Coupling of erbium dopants to yttrium orthosilicate photonic crystal cavities for on-chip optical quantum memories, Evan Miyazono, Tian Zhong, Ioana Craiciu, Jonathan M Kindem, Andrei Faraon, *Applied Physics Letters* 108, 011111 (2016)
2. Coupling erbium dopants in yttrium orthosilicate to silicon photonic resonators and waveguides , Evan Miyazono, Ioana Craiciu, Amir Arbabi, Tian Zhong, Andrei Faraon, *Optics Express* Vol. 25, Issue 3, pp. 2863-2871 (2017)
3. High quality factor nanophotonic resonators in bulk rare-earth doped crystals, Tian Zhong, Jake Rochman, Jonathan M Kindem, Evan Miyazono, Andrei Faraon, *Optics Express* Vol. 24, Issue 1, pp. 536-544 (2016)
4. Nanophotonic rare-earth quantum memory with optically controlled retrieval, Tian Zhong, Jonathan M. Kindem, John G. Bartholomew, Jake Rochman, Ioana Craiciu, Evan Miyazono, Marco Bettinelli, Enrico Cavalli, Varun Verma, Sae Woo Nam, Francesco Marsili, Matthew D. Shaw, Andrew D. Beyer, Andrei Faraon, *Science* 31 Aug 2017: doi:10.1126/science. aan5959 (2017)
5. Engineering and mapping nanocavity emission via precision placement of DNA origami, Ashwin Gopinath, Evan Miyazono, Andrei Faraon, Paul W. K. Rothmund, *Nature*, DOI:10.1038/nature18287 (2016)
6. Nanophotonic quantum storage at telecommunications wavelength, Ioana Craiciu, Mi Lei, Jake Rochman, Jonathan M. Kindem, John Bartholomew, Evan Miyazono, Tian Zhong, Neil Sinclair, and Andrei Faraon, under review in *Physical Review Letters*

# Technical Report: Nanophotonic quantum storage at telecommunications wavelength

## Abstract

Quantum memories for light are important components for future long distance quantum networks. We present on-chip quantum storage of telecommunications band light at the single photon level in an ensemble of erbium-167 ions in an yttrium orthosilicate photonic crystal nanobeam resonator. Storage times of up to  $10 \mu\text{s}$  are demonstrated using an all-optical atomic frequency comb protocol at dilution refrigerator temperatures under a magnetic field of 380 mT. We show this quantum storage platform to have high bandwidth, high fidelity, and multimode capacity, and we outline a path towards an efficient erbium-167 quantum memory for light.

Optical quantum memories can aid processes involving the transfer of quantum information by synchronizing the arrival of photons from multiple channels, with applications in long distance quantum communication and quantum information processing [1–5]. Rare-earth ions in crystals are a promising solid-state platform for optical quantum memories due to their long-lived optical and spin transitions that are highly coherent at cryogenic temperatures [6, 7]. Among rare-earth ions, only erbium has been shown to possess highly coherent optical transitions in the telecommunications band, which allows for integration of memory systems with low loss optical fibers and integrated silicon photonics [8, 9].

Fixed delay quantum storage for less than 50 ns at telecommunications wavelengths has been demonstrated in erbium-doped fibers [10], and erbium-doped lithium niobate waveguides [11] at efficiencies approaching 1%. The protocol used in both cases, the atomic frequency comb (AFC), requires spectrally selective optical pumping, and their efficiencies were limited in part by the lack of a long-lived shelving state in the erbium ions in these hosts. Moving to another crystal host, such as yttrium orthosilicate (YSO) offers the prospect of long-lived shelving states for memory protocols using spectral tailoring of inhomogeneously broadened ensembles including AFC [12] and controlled reversible inhomogeneous broadening (CRIB)[13]. While several optical storage protocols have been realized erbium-doped YSO [14–16], including efficiencies approaching 50% at storage times of 16  $\mu$ s (revival of silenced echo protocol [16]) quantum storage has yet to be demonstrated.

In this work, we demonstrate on-chip quantum storage of telecommunications light at the single photon level. We used a nanophotonic crystal cavity milled directly in  $^{167}\text{Er}^{3+}$  doped YSO ( $^{167}\text{Er}^{3+}:\text{YSO}$ ) to couple to an ensemble of erbium ions and realize quantum storage using the AFC protocol. By working at a temperature of 25 mK and using permanent magnets to apply a field of 380 mT, we accessed a regime in which the ions have optical coherence times of  $\sim 150 \mu$ s and long lived spin states to allow spectral tailoring. We measured storage for up to 10  $\mu$ s. For the shortest measured storage time of 165 ns, we achieved an efficiency of 0.2%, and lower efficiency for longer storage times. We demonstrated storage of multiple temporal modes and measured a high fidelity of storage, exceeding the classical limit. Lastly, we identified the limits on the storage efficiency and proposed avenues for overcoming them to achieve an efficient  $^{167}\text{Er}^{3+}$  quantum memory for light.

Memories using spectral tailoring such as the AFC and CRIB protocols require a long-lived level within the optical ground state manifold, where population can be shelved. Hy-

perfine levels in the optical ground state in  $^{167}\text{Er}^{3+}:\text{YSO}$  have been shown to have long lifetimes at low temperatures and a magnetic field of 7 T [9]. In general, these levels can be long-lived when the erbium electron spin is frozen, which occurs when  $\hbar\omega_e \gg k_B T$ , where  $\omega_e$  is the electron Zeeman splitting [9]. In this work, we satisfied this inequality by using a moderate magnetic field of 380 mT parallel to the  $D_1$  axis of the crystal ( $\omega_e = 2\pi \times 80$  GHz) and a temperature of 25 mK. Under these conditions, the hyperfine lifetime was measured to be 29 minutes, enabling the long-lived, spectrally selective optical pumping required for the AFC protocol (see supplementary material [17]).

Figures 1a-c describe the nanoresonator used in this experiment. A triangular nanobeam photonic crystal cavity [18] was milled in a YSO crystal doped with isotopically purified  $^{167}\text{Er}^{3+}$  (92% purity) at a nominal concentration of 50 ppm. The width of the nanobeam was  $1.5 \mu\text{m}$ , and the length  $\sim 20 \mu\text{m}$ . The slots in the nanobeam created a photonic crystal bandgap, and the periodic pattern (lattice constant = 590 nm, groove width = 450 nm) was modified quadratically in the center to create a cavity mode. Figure 1a shows a scanning electron micrograph of the device and Fig. 1b shows a finite element analysis simulation of the TM cavity mode.

The coherence time of the 1539 nm optical transition, which provides an upper bound on all-optical storage time, was measured to be  $149 \mu\text{s} \pm 4 \mu\text{s}$  in the device. The bulk optical coherence time of this transition under nominally identical cooling conditions was measured to be  $760 \mu\text{s} \pm 41 \mu\text{s}$ . The reduction in coherence time as measured in the device is likely caused by a combination of higher temperature in the nanodevice during measurement and the impact of the focused ion beam milling process [17]. We note that the fabrication method has not significantly impacted the coherence properties of ions in similar devices [19, 20], although the bulk crystal coherence times measured in those works were also lower, preventing a direct comparison to the present case. The optical coherence time did not limit the storage time achieved in this work.

Figure 1d shows a schematic of the optical testing setup. Figure 1c shows the reflection spectrum of the nanobeam cavity, which has a measured loaded quality factor of  $7 \times 10^3$ . The cavity was tuned onto resonance with the 1539 nm transition of the  $^{167}\text{Er}^{3+}$  ions by freezing nitrogen gas onto the nanobeam at cryogenic temperatures [21]. The coupling of the ensemble of ions to the cavity is seen as a peak in the cavity reflection dip. The inset shows a close-up of the ion-cavity coupling (in black) and a fit to theory [22]. The ensemble

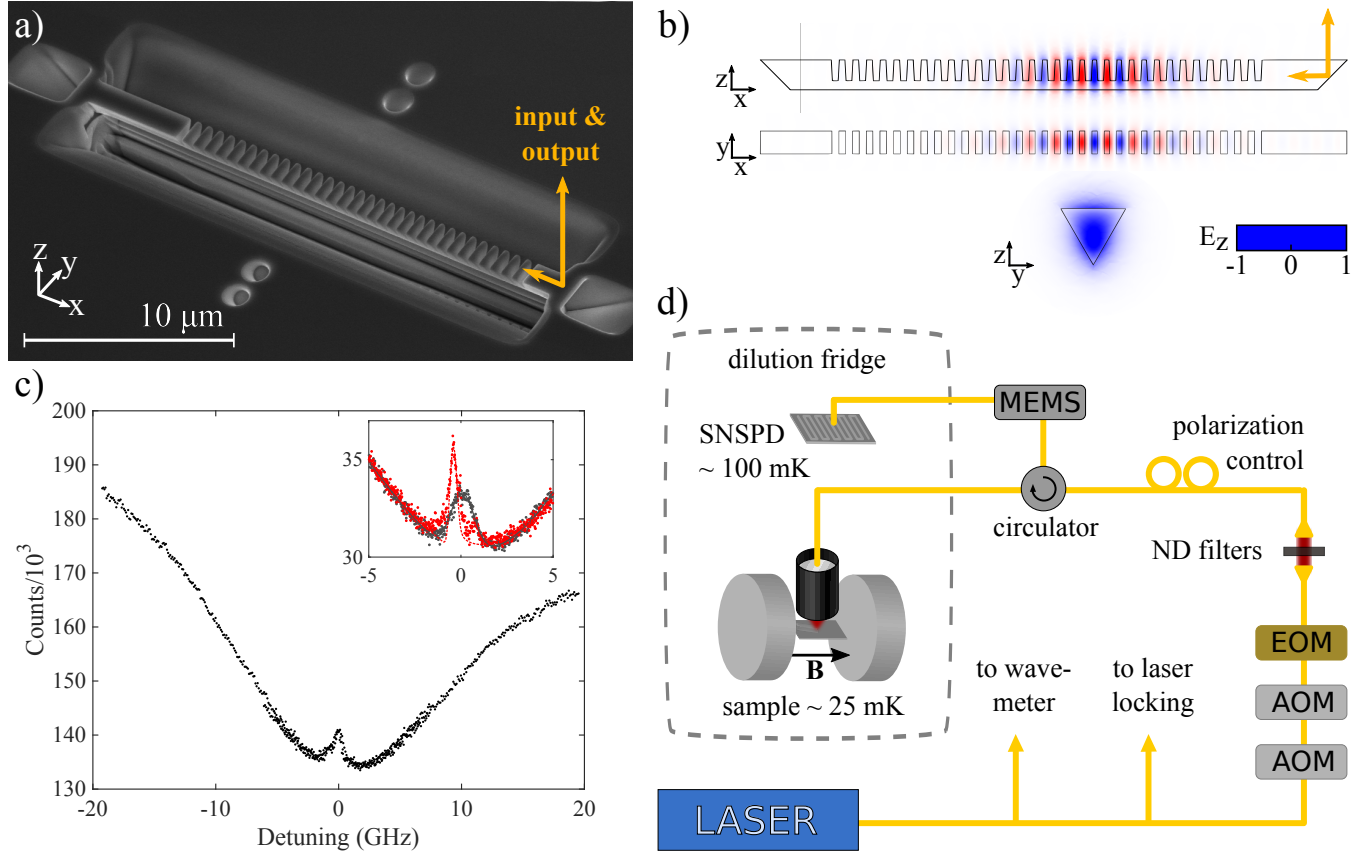


FIG. 1. (a) Scanning electron micrograph of the triangular nanobeam resonator, showing input/output coupling through a  $45^\circ$  angled slot coupler, which used total internal reflection to couple light into the nanobeam. (b) Simulation of the TM cavity mode. Red-blue color gradient indicates the electric field component normal to the surface,  $E_z$ ; black outline indicates YSO-air interface; yellow arrows indicate coupling. (c) Reflection spectrum of cavity when tuned on resonance to the  $1539\text{ nm }^{167}\text{Er}^{3+}:\text{YSO}$  transition. Detuning is measured from  $194816\text{ GHz} \pm 2\text{ GHz}$ . Inset shows a close-up of ion coupling before (black) and after (red) partial hyperfine initialization. Circles are data points and lines (black solid and red dashed) are fits to theory (see main text for details). (d) Schematic of setup. Light from an external-cavity diode laser was directed through two acousto-optical modulators (AOMs) for pulse shaping. An electro-optic phase modulator (EOM) was used to generate strong sidebands necessary for initialization. Neutral density (ND) filters and polarization paddles provided attenuation and polarization control, respectively. A circulator directed light to the  $^{167}\text{Er}^{3+}:\text{YSO}$  crystal located inside a dilution refrigerator, nominally at  $25\text{ mK}$ . An aspheric lens pair focused light from an optical fiber onto the angled coupler of the resonator. Light from the resonator was directed by the circulator onto a superconducting nanowire single photon detector at  $\sim 100\text{ mK}$ . A magnetic field  $\mathbf{B} = 380\text{ mT}$  was applied to the sample using two cylindrical permanent magnets. More details are in the supplementary material [17].

cooperativity was estimated from the fit to this curve to be 0.1 [17]. For high efficiency storage using ions coupled to a cavity, the ensemble cooperativity (after spectral tailoring) should equal one [23, 24]. An increased ensemble cooperativity of 0.3, as shown in red in the inset of Fig. 1c, was obtained using a partial hyperfine initialization procedure. The spectral density of erbium ions in the center of the inhomogeneous line (zero detuning) was increased from its thermal equilibrium value by sweeping the laser frequency between 350 MHz and 820 MHz on both sides of the inhomogeneous line. This procedure can be optimized to further increase the ensemble cooperativity, but was limited here by the relatively weak magnetic field, which allows only partial hyperfine initialization [17]. At 7 T, initialization into one hyperfine state with an efficiency of 95% has been demonstrated[9].

The nanobeam device was used to demonstrate quantum optical storage using the AFC protocol [12]. In this protocol, a pulse of light that is absorbed by an atomic frequency comb with an inter-tooth spacing of  $\Delta$  is stored for  $t = 1/\Delta$ . Frequency selective optical pumping was used to create a frequency comb within the inhomogeneous linewidth, as shown in Fig. 2a. Figure 2b shows a schematic of the protocol, from hyperfine initialization, through comb creation, to storage of weak coherent pulses. First, a long pulse with strong frequency modulated sidebands was used for partial hyperfine initialization. The next 15 pulses, repeated  $n_{\text{pump}} = 60$  times, created the comb; the laser frequency was swept through 15 values, separated by  $\Delta = 6.1$  MHz, to optically pump away ions and create 15 spectral transparencies. The following  $n_{\text{input}} = 60$  pulses were zero detuning weak coherent states which were stored in the frequency comb. The full experiment was repeated  $\sim 10^4$  times. As shown in Fig. 2c, 60 ns wide pulses with an average photon number of  $\bar{n} = 0.60 \pm 0.09$  were stored for 165 ns with an efficiency of 0.2%. Despite the partial initialization, the storage efficiency was limited by the ensemble cooperativity of the device [17].

Coherent pulses could be stored in the device for up to 10  $\mu\text{s}$ , although with lower efficiency, as shown in Fig. 3. For this experiment, as for all storage times longer than 165 ns, we used an accumulated AFC method [17, 25] to create the comb. As shown in the inset of Fig. 3, weak pairs of pulses separated by  $t_{\text{storage}} = 10 \mu\text{s}$  were repeatedly sent into the cavity. The Fourier transform of each pulse pair is a frequency comb, which imprinted onto the  $^{167}\text{Er}^{3+}$  inhomogeneous line to create the AFC. The efficiency at this long storage time was limited by laser frequency jitter and by superhyperfine coupling to the yttrium ions in YSO. Superhyperfine coupling limits the narrowest spectral feature to  $\sim 1$  MHz

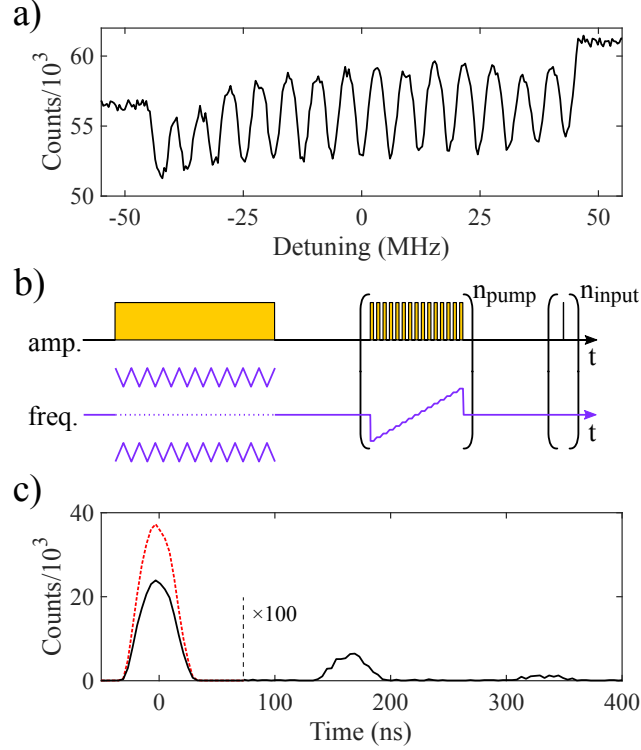


FIG. 2. (Color online) Atomic frequency comb experiment in the nanobeam cavity. (a) A section of the resonator reflection spectrum, showing an atomic frequency comb in the center of the inhomogeneously broadened  $^{167}\text{Er}^{3+}$  transition. Detuning is measured from  $194814.2 \text{ GHz} \pm 0.1 \text{ GHz}$ . The apparent slope of the comb is due to its center frequency not being precisely aligned to the cavity resonance, leading to a dispersive shape. (b) Schematic of AFC pulse sequence showing amplitude (yellow) and frequency (purple) modulation of the laser. The pulse widths and heights are not drawn to scale. The details of the sequence are described in the main text. (c) AFC storage: the input pulse (red dashed line) was partially absorbed by the comb and an output (stored) pulse was emitted at time  $1/\Delta = 165 \text{ ns}$ . The black line shows the partially reflected input pulse and the output pulse intensity ( $\times 100$ ). A smaller second output pulse is seen at 330 ns.

[26, 27], which exceeds the maximum width of the comb features needed for this storage time:  $\Delta = 1/t_{\text{storage}} = 0.1 \text{ MHz}$ .

The AFC protocol is capable of storing multiple temporal modes [12]. Ten coherent pulses were stored in this device, as shown in Fig. 4a. Multiplexing in frequency is also possible [28]. The AFC comb in Figure 2a has a bandwidth of  $\sim 90 \text{ MHz}$  (see Fig. 2a) which can accommodate storage in multiple frequency modes, for example nine 50 ns pulses.

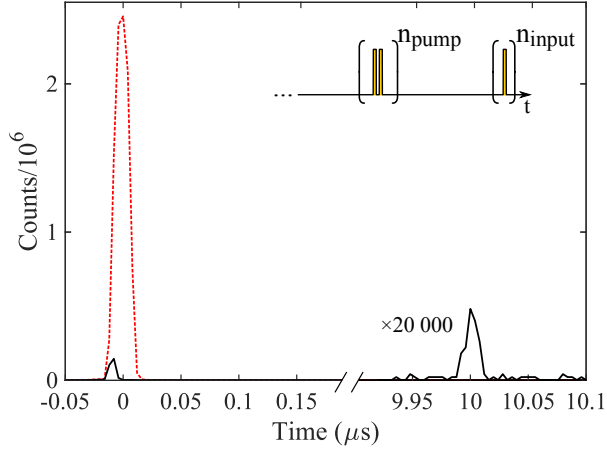


FIG. 3. (Color online) AFC storage for 10  $\mu\text{s}$  in the nanobeam resonator. Red dashed line shows the input pulse. Black line shows the partially reflected input pulse and the output pulse ( $\times 20\,000$ ). The reflected input pulse appears small due to detector saturation. Inset shows a schematic of the pulse sequence following hyperfine initialization. Pairs of comb preparation pulses 10  $\mu\text{s}$  apart were repeated  $n_{\text{pump}} = 10\,000$  times, followed by input pulses 20 ns wide repeated  $n_{\text{input}} = 10$  times.

An inhomogeneous linewidth of 150 MHz limits the bandwidth of storage in this system. Although there exist methods to increase this linewidth [29], the bandwidth cannot be increased much further before being limited by overlapping optical transitions from other hyperfine levels.

In quantum storage protocols, the phase coherence of the stored state must be preserved. A double atomic frequency comb experiment was used to characterize the coherence of the storage process [25]. Two overlapping spectral combs with tooth spacing  $\Delta_1, \Delta_2$  and with frequency detuning  $\delta_1, \delta_2$ , were created, so that each input pulse was mapped to two output pulses at times  $1/\Delta_1, 1/\Delta_2$  and with a relative phase  $\phi_{\text{rel}} = 2\pi \left( \frac{\delta_2}{\Delta_2} - \frac{\delta_1}{\Delta_1} \right)$  [12]. An input state encoded into two pulses,  $|\psi_{\text{in}}\rangle = \frac{1}{\sqrt{2}} (|\text{early}\rangle + |\text{late}\rangle)$ , was therefore mapped to a total of four output pulses. By appropriately selecting the time interval between the early and late input pulses, two of the four output pulses were made to overlap and either constructively or destructively interfere, depending on  $\phi_{\text{rel}}$  (see inset of Fig. 4b). Using an input state with mean photon number  $\bar{n} = 0.6 \pm 0.09$ , and sweeping  $\phi_{\text{rel}}$  via the detuning  $\delta_2$ , the interference fringe shown in Fig. 4b was obtained (see caption for details). The double comb acted as an interferometer, where the early and late input pulses interfered post-storage. The measured

visibility of  $91.2\% \pm 3.4\%$  demonstrates the high degree of coherence of this on-chip storage process. The visibility was limited by the 12 counts in the total destructive interference case ( $\delta_2 = \frac{\Delta_2}{2} \rightarrow \phi_{\text{rel}} = \pi$ ). This was due in part to imperfect cancellation of the two overlapping output pulses, resulting from the slightly different efficiencies of storage in the two atomic frequency combs, and in part to a dark count rate of 18.5 Hz, which lead to a baseline of 7 counts. The dark-count-subtracted visibility is  $97.0\% \pm 3.6\%$ .

The double comb method was also used to estimate a lower bound for the fidelity of storing single photon time bin states,  $F^{(n=1)}$ . The fidelity of storage was measured for four input states  $|\text{early}\rangle$ ,  $|\text{late}\rangle$ ,  $\frac{|\text{early}\rangle+|\text{late}\rangle}{\sqrt{2}}$  and  $\frac{|\text{early}\rangle-|\text{late}\rangle}{\sqrt{2}}$ , using two mean photon numbers

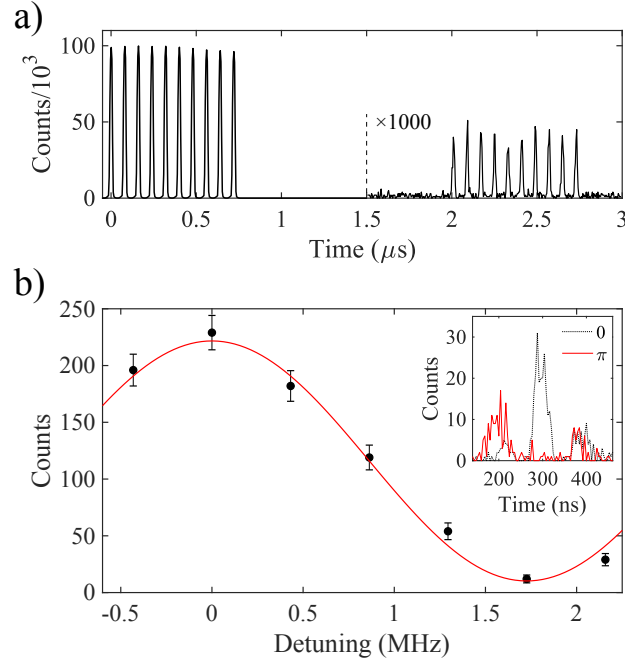


FIG. 4. (Color online) Multimode and coherent storage using the AFC protocol in the nanobeam resonator. (a) Storage of multiple temporal modes: ten 20 ns wide input pulses (reflection off cavity shown) and the corresponding 10 output pulses from a 500 kHz AFC ( $\times 1000$ ). (b) Visibility curve acquired using double comb experiment, with  $\Delta_1 = 5.2$  MHz,  $\Delta_2 = 3.4$  MHz,  $\delta_1 = 0$  MHz. The detuning of the second comb was swept from  $\delta_2 = -0.2$  MHz to  $\delta_2 = 2.2$  MHz, and the intensity of the two central overlapping output pulses was measured. Black circles show the sum of counts in the overlapping pulse region with  $\sqrt{N_{\text{counts}}}$  uncertainty bars. Red line shows a least squares fit to a sinusoid. Inset shows the four output pulses (middle two overlapping) in the case of the maximally constructive (black dashed line) and maximally destructive (red line) interference.

$\bar{n} = 0.30$  and  $\bar{n} = 0.60$ . With these values, the decoy state method [17, 28, 30] was used to calculate a bound on the fidelity for storing single photon states  $F^{(n=1)} \geq 93.7\% \pm 2.4\%$ , which exceeds the classical limit of  $F = 2/3$ . Similar to the case for visibility discussed above, the measured fidelity was limited in part by dark counts and in part by the double comb protocol being an imperfect interferometer [17].

While the storage presented here was limited in efficiency, a nanophotonic cavity coupled to  $^{167}\text{Er}^{3+}$  ions in YSO promises to be an efficient quantum storage system. The main limitations to the storage efficiency in this work were a low ensemble cooperativity of 0.3 and loss from the optical nanobeam cavity. The cooperativity can be increased using higher  $^{167}\text{Er}^{3+}$  doping and better hyperfine initialization, which would require increasing the applied magnetic field or changing its angle [9, 17]. A higher intrinsic quality factor resonator would serve to both increase cooperativity and decrease cavity loss. For example, using a YSO crystal with 200 ppm  $^{167}\text{Er}^{3+}$  doping, optimal hyperfine initialization, and a resonator with an intrinsic quality factor of 2 million, the theoretical efficiency of the AFC quantum storage is 90% (see supplementary material for analysis [17]). Using a silicon resonator evanescently coupled to  $^{167}\text{Er}^{3+}$  ions in YSO [8, 31] would allow leveraging mature silicon nanofabrication technology to achieve this goal. With this efficiency level and a storage time of  $10 \mu\text{s}$ , the device would outperform standard telecommunications fiber [32], an important measure of success for optical quantum memories. With the optical AFC protocol alone, it may be difficult to achieve efficient storage for this duration due to the limit on narrowness of spectral features set by superhyperfine coupling. However, the AFC spin-wave protocol, where the stored information is reversibly transferred from the optical to the hyperfine manifold [12], would enable even longer storage without the same requirements for narrow spectral features, as well as adding on-demand recall capability. The availability of hyperfine states with coherence times exceeding 1 second [9] make  $^{167}\text{Er}^{3+}:\text{YSO}$  a promising system for spin-wave storage.

In conclusion, we have demonstrated on-chip quantum storage of telecommunications band light at the single photon level. The storage had a bandwidth of  $\sim 90 \text{ MHz}$ , and a storage fidelity for single photon states of at least  $93.7\% \pm 2.4\%$ .  $^{167}\text{Er}^{3+}:\text{YSO}$  at dilution refrigerator temperatures and moderate magnetic field was shown to be a promising material for AFC quantum memories. A clear path exists for creating a high efficiency quantum

memory using this material and a nanoscale resonator.

---

- [1] H. J. Kimble, *Nature* **453**, 1023 (2008).
- [2] K. Heshami, D. G. England, P. C. Humphreys, P. J. Bustard, V. M. Acosta, J. Nunn, and B. J. Sussman, *Journal of Modern Optics* **63**, 2005 (2016).
- [3] H.-J. Briegel, W. Dür, J. I. Cirac, and P. Zoller, *Phys. Rev. Lett.* **81**, 5932 (1998).
- [4] P. Kok, W. J. Munro, K. Nemoto, T. C. Ralph, J. P. Dowling, and G. J. Milburn, *Rev. Mod. Phys.* **79**, 135 (2007).
- [5] C. Monroe, R. Raussendorf, A. Ruthven, K. R. Brown, P. Maunz, L.-M. Duan, and J. Kim, *Phys. Rev. A* **89**, 022317 (2014).
- [6] C. Thiel, T. Böttger, and R. Cone, *Journal of Luminescence* **131**, 353 (2011).
- [7] M. Zhong, M. P. Hedges, R. L. Ahlefeldt, J. G. Bartholomew, S. E. Beavan, S. M. Wittig, J. J. Longdell, and M. J. Sellars, *Nature* **517**, 177 (2015).
- [8] E. Miyazono, I. Craiciu, A. Arbabi, T. Zhong, and A. Faraon, *Opt. Express* **25**, 2863 (2017).
- [9] M. Rančić, M. P. Hedges, R. L. Ahlefeldt, and M. J. Sellars, *Nature Physics* **14**, 50 (2018).
- [10] E. Saglamyurek, J. Jin, V. B. Verma, M. D. Shaw, F. Marsili, S. W. Nam, D. Oblak, and W. Tittel, *Nature Photonics* **9**, 83 (2015).
- [11] M. F. Askarani, M. G. Pugibert, T. Lutz, V. B. Verma, M. D. Shaw, S. W. Nam, N. Sinclair, D. Oblak, and W. Tittel, (2018), arXiv:<https://arxiv.org/abs/1804.05699>.
- [12] M. Afzelius, C. Simon, H. de Riedmatten, and N. Gisin, *Phys. Rev. A* **79**, 052329 (2009).
- [13] M. Nilsson and S. Kröll, *Optics Communications* **247**, 393 (2005).
- [14] B. Lauritzen, J. Minář, H. de Riedmatten, M. Afzelius, N. Sangouard, C. Simon, and N. Gisin, *Phys. Rev. Lett.* **104**, 080502 (2010).
- [15] B. Lauritzen, J. Minář, H. de Riedmatten, M. Afzelius, and N. Gisin, *Phys. Rev. A* **83**, 012318 (2011).
- [16] J. Dajczgewand, J.-L. L. Gouët, A. Louchet-Chauvet, and T. Chanelière, *Opt. Lett.* **39**, 2711 (2014).
- [17] See Supplemental Material at **URL will be inserted by publisher** for material characterization details and calculation of storage cooperativity, fidelity, and efficiency.
- [18] T. Zhong, J. Rochman, J. M. Kindem, E. Miyazono, and A. Faraon, *Opt. Express* **24**, 536

- (2016).
- [19] T. Zhong, J. M. Kindem, E. Miyazono, and A. Faraon, *Nature Communications* **6**, 8206 (2015).
- [20] T. Zhong, J. M. Kindem, J. G. Bartholomew, J. Rochman, I. Craiciu, E. Miyazono, M. Bettinelli, E. Cavalli, V. Verma, S. W. Nam, F. Marsili, M. D. Shaw, A. D. Beyer, and A. Faraon, *Science* (2017), 10.1126/science.aan5959.
- [21] S. Mosor, J. Hendrickson, B. C. Richards, J. Sweet, G. Khitrova, H. M. Gibbs, T. Yoshie, A. Scherer, O. B. Shchekin, and D. G. Deppe, *Applied Physics Letters* **87**, 141105 (2005).
- [22] I. Diniz, S. Portolan, R. Ferreira, J. M. Gérard, P. Bertet, and A. Auffèves, *Phys. Rev. A* **84**, 063810 (2011).
- [23] M. Afzelius and C. Simon, *Phys. Rev. A* **82**, 022310 (2010).
- [24] S. A. Moiseev, S. N. Andrianov, and F. F. Gubaidullin, *Phys. Rev. A* **82**, 022311 (2010).
- [25] H. de Riedmatten, M. Afzelius, M. U. Staudt, C. Simon, and N. Gisin, *Nature* **456**, 773 (2008).
- [26] O. Guillot-Noël, H. Vezin, P. Goldner, F. Beaudoux, J. Vincent, J. Lejay, and I. Lorgeré, *Phys. Rev. B* **76**, 180408 (2007).
- [27] B. Car, L. Veissier, A. Louchet-Chauvet, J.-L. Le Gouët, and T. Chanelière, *Phys. Rev. Lett.* **120**, 197401 (2018).
- [28] N. Sinclair, E. Saglamyurek, H. Mallahzadeh, J. A. Slater, M. George, R. Ricken, M. P. Hedges, D. Oblak, C. Simon, W. Sohler, and W. Tittel, *Phys. Rev. Lett.* **113**, 053603 (2014).
- [29] S. Welinski, C. W. Thiel, J. Dajczgewand, A. Ferrier, R. L. Cone, R. M. Macfarlane, T. Chanelière, A. Louchet-Chauvet, and P. Goldner, *Optical Materials* **63**, 69 (2017).
- [30] X. Ma, B. Qi, Y. Zhao, and H.-K. Lo, *Phys. Rev. A* **72**, 012326 (2005).
- [31] A. M. Dibos, M. Raha, C. M. Phenicie, and J. D. Thompson, *Phys. Rev. Lett.* **120**, 243601 (2018).
- [32] Y.-W. Cho, G. T. Campbell, J. L. Everett, J. Bernu, D. B. Higginbottom, M. T. Cao, J. Geng, N. P. Robins, P. K. Lam, and B. C. Buchler, *Optica* **3**, 100 (2016).

# Technical Report: Nanophotonic quantum storage at telecommunications wavelength

## Abstract

Quantum memories for light are important components for future long distance quantum networks. We present on-chip quantum storage of telecommunications band light at the single photon level in an ensemble of erbium-167 ions in an yttrium orthosilicate photonic crystal nanobeam resonator. Storage times of up to  $10 \mu\text{s}$  are demonstrated using an all-optical atomic frequency comb protocol at dilution refrigerator temperatures under a magnetic field of 380 mT. We show this quantum storage platform to have high bandwidth, high fidelity, and multimode capacity, and we outline a path towards an efficient erbium-167 quantum memory for light.

Optical quantum memories can aid processes involving the transfer of quantum information by synchronizing the arrival of photons from multiple channels, with applications in long distance quantum communication and quantum information processing [1–5]. Rare-earth ions in crystals are a promising solid-state platform for optical quantum memories due to their long-lived optical and spin transitions that are highly coherent at cryogenic temperatures [6, 7]. Among rare-earth ions, only erbium has been shown to possess highly coherent optical transitions in the telecommunications band, which allows for integration of memory systems with low loss optical fibers and integrated silicon photonics [8, 9].

Fixed delay quantum storage for less than 50 ns at telecommunications wavelengths has been demonstrated in erbium-doped fibers [10], and erbium-doped lithium niobate waveguides [11] at efficiencies approaching 1%. The protocol used in both cases, the atomic frequency comb (AFC), requires spectrally selective optical pumping, and their efficiencies were limited in part by the lack of a long-lived shelving state in the erbium ions in these hosts. Moving to another crystal host, such as yttrium orthosilicate (YSO) offers the prospect of long-lived shelving states for memory protocols using spectral tailoring of inhomogeneously broadened ensembles including AFC [12] and controlled reversible inhomogeneous broadening (CRIB)[13]. While several optical storage protocols have been realized erbium-doped YSO [14–16], including efficiencies approaching 50% at storage times of 16  $\mu$ s (revival of silenced echo protocol [16]) quantum storage has yet to be demonstrated.

In this work, we demonstrate on-chip quantum storage of telecommunications light at the single photon level. We used a nanophotonic crystal cavity milled directly in  $^{167}\text{Er}^{3+}$  doped YSO ( $^{167}\text{Er}^{3+}:\text{YSO}$ ) to couple to an ensemble of erbium ions and realize quantum storage using the AFC protocol. By working at a temperature of 25 mK and using permanent magnets to apply a field of 380 mT, we accessed a regime in which the ions have optical coherence times of  $\sim 150 \mu$ s and long lived spin states to allow spectral tailoring. We measured storage for up to 10  $\mu$ s. For the shortest measured storage time of 165 ns, we achieved an efficiency of 0.2%, and lower efficiency for longer storage times. We demonstrated storage of multiple temporal modes and measured a high fidelity of storage, exceeding the classical limit. Lastly, we identified the limits on the storage efficiency and proposed avenues for overcoming them to achieve an efficient  $^{167}\text{Er}^{3+}$  quantum memory for light.

Memories using spectral tailoring such as the AFC and CRIB protocols require a long-lived level within the optical ground state manifold, where population can be shelved. Hy-

perfine levels in the optical ground state in  $^{167}\text{Er}^{3+}:\text{YSO}$  have been shown to have long lifetimes at low temperatures and a magnetic field of 7 T [9]. In general, these levels can be long-lived when the erbium electron spin is frozen, which occurs when  $\hbar\omega_e \gg k_B T$ , where  $\omega_e$  is the electron Zeeman splitting [9]. In this work, we satisfied this inequality by using a moderate magnetic field of 380 mT parallel to the  $D_1$  axis of the crystal ( $\omega_e = 2\pi \times 80$  GHz) and a temperature of 25 mK. Under these conditions, the hyperfine lifetime was measured to be 29 minutes, enabling the long-lived, spectrally selective optical pumping required for the AFC protocol (see supplementary material [17]).

Figures 1a-c describe the nanoresonator used in this experiment. A triangular nanobeam photonic crystal cavity [18] was milled in a YSO crystal doped with isotopically purified  $^{167}\text{Er}^{3+}$  (92% purity) at a nominal concentration of 50 ppm. The width of the nanobeam was  $1.5 \mu\text{m}$ , and the length  $\sim 20 \mu\text{m}$ . The slots in the nanobeam created a photonic crystal bandgap, and the periodic pattern (lattice constant = 590 nm, groove width = 450 nm) was modified quadratically in the center to create a cavity mode. Figure 1a shows a scanning electron micrograph of the device and Fig. 1b shows a finite element analysis simulation of the TM cavity mode.

The coherence time of the 1539 nm optical transition, which provides an upper bound on all-optical storage time, was measured to be  $149 \mu\text{s} \pm 4 \mu\text{s}$  in the device. The bulk optical coherence time of this transition under nominally identical cooling conditions was measured to be  $760 \mu\text{s} \pm 41 \mu\text{s}$ . The reduction in coherence time as measured in the device is likely caused by a combination of higher temperature in the nanodevice during measurement and the impact of the focused ion beam milling process [17]. We note that the fabrication method has not significantly impacted the coherence properties of ions in similar devices [19, 20], although the bulk crystal coherence times measured in those works were also lower, preventing a direct comparison to the present case. The optical coherence time did not limit the storage time achieved in this work.

Figure 1d shows a schematic of the optical testing setup. Figure 1c shows the reflection spectrum of the nanobeam cavity, which has a measured loaded quality factor of  $7 \times 10^3$ . The cavity was tuned onto resonance with the 1539 nm transition of the  $^{167}\text{Er}^{3+}$  ions by freezing nitrogen gas onto the nanobeam at cryogenic temperatures [21]. The coupling of the ensemble of ions to the cavity is seen as a peak in the cavity reflection dip. The inset shows a close-up of the ion-cavity coupling (in black) and a fit to theory [22]. The ensemble

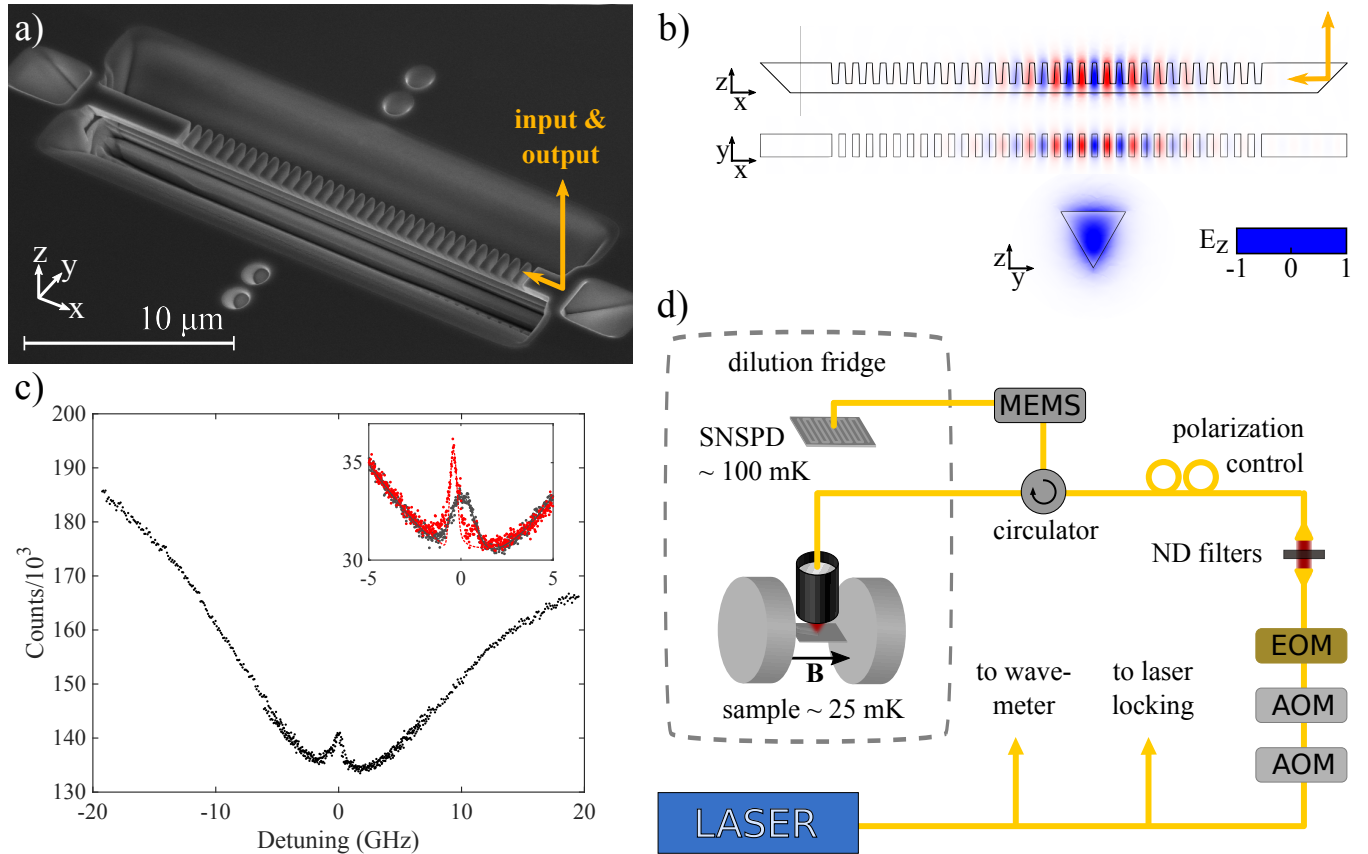


FIG. 1. (a) Scanning electron micrograph of the triangular nanobeam resonator, showing input/output coupling through a  $45^\circ$  angled slot coupler, which used total internal reflection to couple light into the nanobeam. (b) Simulation of the TM cavity mode. Red-blue color gradient indicates the electric field component normal to the surface,  $E_z$ ; black outline indicates YSO-air interface; yellow arrows indicate coupling. (c) Reflection spectrum of cavity when tuned on resonance to the  $1539\text{ nm }^{167}\text{Er}^{3+}:\text{YSO}$  transition. Detuning is measured from  $194816\text{ GHz} \pm 2\text{ GHz}$ . Inset shows a close-up of ion coupling before (black) and after (red) partial hyperfine initialization. Circles are data points and lines (black solid and red dashed) are fits to theory (see main text for details). (d) Schematic of setup. Light from an external-cavity diode laser was directed through two acousto-optical modulators (AOMs) for pulse shaping. An electro-optic phase modulator (EOM) was used to generate strong sidebands necessary for initialization. Neutral density (ND) filters and polarization paddles provided attenuation and polarization control, respectively. A circulator directed light to the  $^{167}\text{Er}^{3+}:\text{YSO}$  crystal located inside a dilution refrigerator, nominally at  $25\text{ mK}$ . An aspheric lens pair focused light from an optical fiber onto the angled coupler of the resonator. Light from the resonator was directed by the circulator onto a superconducting nanowire single photon detector at  $\sim 100\text{ mK}$ . A magnetic field  $\mathbf{B} = 380\text{ mT}$  was applied to the sample using two cylindrical permanent magnets. More details are in the supplementary material [17].

cooperativity was estimated from the fit to this curve to be 0.1 [17]. For high efficiency storage using ions coupled to a cavity, the ensemble cooperativity (after spectral tailoring) should equal one [23, 24]. An increased ensemble cooperativity of 0.3, as shown in red in the inset of Fig. 1c, was obtained using a partial hyperfine initialization procedure. The spectral density of erbium ions in the center of the inhomogeneous line (zero detuning) was increased from its thermal equilibrium value by sweeping the laser frequency between 350 MHz and 820 MHz on both sides of the inhomogeneous line. This procedure can be optimized to further increase the ensemble cooperativity, but was limited here by the relatively weak magnetic field, which allows only partial hyperfine initialization [17]. At 7 T, initialization into one hyperfine state with an efficiency of 95% has been demonstrated[9].

The nanobeam device was used to demonstrate quantum optical storage using the AFC protocol [12]. In this protocol, a pulse of light that is absorbed by an atomic frequency comb with an inter-tooth spacing of  $\Delta$  is stored for  $t = 1/\Delta$ . Frequency selective optical pumping was used to create a frequency comb within the inhomogeneous linewidth, as shown in Fig. 2a. Figure 2b shows a schematic of the protocol, from hyperfine initialization, through comb creation, to storage of weak coherent pulses. First, a long pulse with strong frequency modulated sidebands was used for partial hyperfine initialization. The next 15 pulses, repeated  $n_{\text{pump}} = 60$  times, created the comb; the laser frequency was swept through 15 values, separated by  $\Delta = 6.1$  MHz, to optically pump away ions and create 15 spectral transparencies. The following  $n_{\text{input}} = 60$  pulses were zero detuning weak coherent states which were stored in the frequency comb. The full experiment was repeated  $\sim 10^4$  times. As shown in Fig. 2c, 60 ns wide pulses with an average photon number of  $\bar{n} = 0.60 \pm 0.09$  were stored for 165 ns with an efficiency of 0.2%. Despite the partial initialization, the storage efficiency was limited by the ensemble cooperativity of the device [17].

Coherent pulses could be stored in the device for up to 10  $\mu\text{s}$ , although with lower efficiency, as shown in Fig. 3. For this experiment, as for all storage times longer than 165 ns, we used an accumulated AFC method [17, 25] to create the comb. As shown in the inset of Fig. 3, weak pairs of pulses separated by  $t_{\text{storage}} = 10 \mu\text{s}$  were repeatedly sent into the cavity. The Fourier transform of each pulse pair is a frequency comb, which imprinted onto the  $^{167}\text{Er}^{3+}$  inhomogeneous line to create the AFC. The efficiency at this long storage time was limited by laser frequency jitter and by superhyperfine coupling to the yttrium ions in YSO. Superhyperfine coupling limits the narrowest spectral feature to  $\sim 1$  MHz

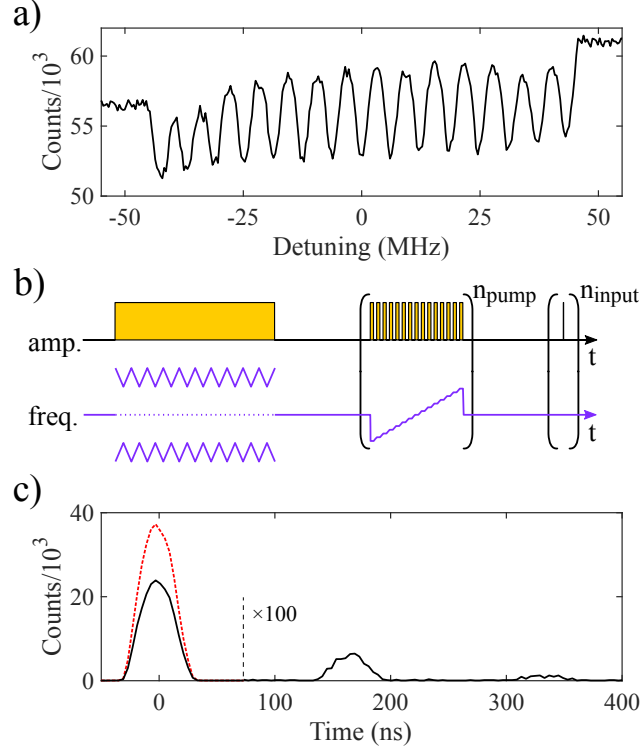


FIG. 2. (Color online) Atomic frequency comb experiment in the nanobeam cavity. (a) A section of the resonator reflection spectrum, showing an atomic frequency comb in the center of the inhomogeneously broadened  $^{167}\text{Er}^{3+}$  transition. Detuning is measured from  $194814.2 \text{ GHz} \pm 0.1 \text{ GHz}$ . The apparent slope of the comb is due to its center frequency not being precisely aligned to the cavity resonance, leading to a dispersive shape. (b) Schematic of AFC pulse sequence showing amplitude (yellow) and frequency (purple) modulation of the laser. The pulse widths and heights are not drawn to scale. The details of the sequence are described in the main text. (c) AFC storage: the input pulse (red dashed line) was partially absorbed by the comb and an output (stored) pulse was emitted at time  $1/\Delta = 165 \text{ ns}$ . The black line shows the partially reflected input pulse and the output pulse intensity ( $\times 100$ ). A smaller second output pulse is seen at 330 ns.

[26, 27], which exceeds the maximum width of the comb features needed for this storage time:  $\Delta = 1/t_{\text{storage}} = 0.1 \text{ MHz}$ .

The AFC protocol is capable of storing multiple temporal modes [12]. Ten coherent pulses were stored in this device, as shown in Fig. 4a. Multiplexing in frequency is also possible [28]. The AFC comb in Figure 2a has a bandwidth of  $\sim 90 \text{ MHz}$  (see Fig. 2a) which can accommodate storage in multiple frequency modes, for example nine 50 ns pulses.

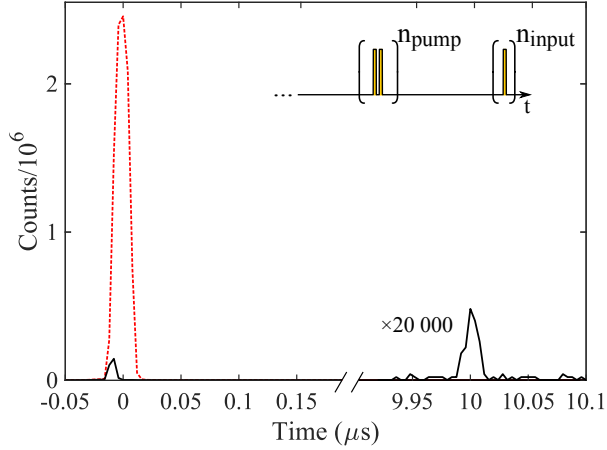


FIG. 3. (Color online) AFC storage for 10  $\mu\text{s}$  in the nanobeam resonator. Red dashed line shows the input pulse. Black line shows the partially reflected input pulse and the output pulse ( $\times 20\,000$ ). The reflected input pulse appears small due to detector saturation. Inset shows a schematic of the pulse sequence following hyperfine initialization. Pairs of comb preparation pulses 10  $\mu\text{s}$  apart were repeated  $n_{\text{pump}} = 10\,000$  times, followed by input pulses 20 ns wide repeated  $n_{\text{input}} = 10$  times.

An inhomogeneous linewidth of 150 MHz limits the bandwidth of storage in this system. Although there exist methods to increase this linewidth [29], the bandwidth cannot be increased much further before being limited by overlapping optical transitions from other hyperfine levels.

In quantum storage protocols, the phase coherence of the stored state must be preserved. A double atomic frequency comb experiment was used to characterize the coherence of the storage process [25]. Two overlapping spectral combs with tooth spacing  $\Delta_1, \Delta_2$  and with frequency detuning  $\delta_1, \delta_2$ , were created, so that each input pulse was mapped to two output pulses at times  $1/\Delta_1, 1/\Delta_2$  and with a relative phase  $\phi_{\text{rel}} = 2\pi \left( \frac{\delta_2}{\Delta_2} - \frac{\delta_1}{\Delta_1} \right)$  [12]. An input state encoded into two pulses,  $|\psi_{\text{in}}\rangle = \frac{1}{\sqrt{2}} (|\text{early}\rangle + |\text{late}\rangle)$ , was therefore mapped to a total of four output pulses. By appropriately selecting the time interval between the early and late input pulses, two of the four output pulses were made to overlap and either constructively or destructively interfere, depending on  $\phi_{\text{rel}}$  (see inset of Fig. 4b). Using an input state with mean photon number  $\bar{n} = 0.6 \pm 0.09$ , and sweeping  $\phi_{\text{rel}}$  via the detuning  $\delta_2$ , the interference fringe shown in Fig. 4b was obtained (see caption for details). The double comb acted as an interferometer, where the early and late input pulses interfered post-storage. The measured

visibility of  $91.2\% \pm 3.4\%$  demonstrates the high degree of coherence of this on-chip storage process. The visibility was limited by the 12 counts in the total destructive interference case ( $\delta_2 = \frac{\Delta_2}{2} \rightarrow \phi_{\text{rel}} = \pi$ ). This was due in part to imperfect cancellation of the two overlapping output pulses, resulting from the slightly different efficiencies of storage in the two atomic frequency combs, and in part to a dark count rate of 18.5 Hz, which lead to a baseline of 7 counts. The dark-count-subtracted visibility is  $97.0\% \pm 3.6\%$ .

The double comb method was also used to estimate a lower bound for the fidelity of storing single photon time bin states,  $F^{(n=1)}$ . The fidelity of storage was measured for four input states  $|\text{early}\rangle$ ,  $|\text{late}\rangle$ ,  $\frac{|\text{early}\rangle+|\text{late}\rangle}{\sqrt{2}}$  and  $\frac{|\text{early}\rangle-|\text{late}\rangle}{\sqrt{2}}$ , using two mean photon numbers

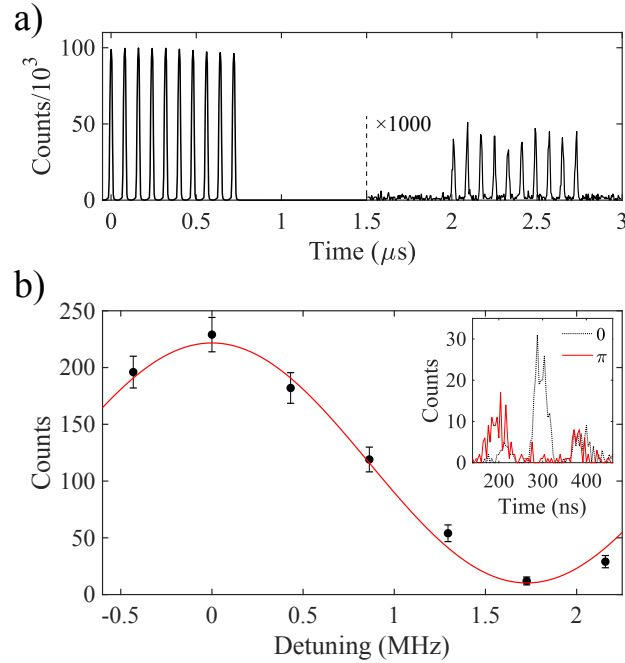


FIG. 4. (Color online) Multimode and coherent storage using the AFC protocol in the nanobeam resonator. (a) Storage of multiple temporal modes: ten 20 ns wide input pulses (reflection off cavity shown) and the corresponding 10 output pulses from a 500 kHz AFC ( $\times 1000$ ). (b) Visibility curve acquired using double comb experiment, with  $\Delta_1 = 5.2$  MHz,  $\Delta_2 = 3.4$  MHz,  $\delta_1 = 0$  MHz. The detuning of the second comb was swept from  $\delta_2 = -0.2$  MHz to  $\delta_2 = 2.2$  MHz, and the intensity of the two central overlapping output pulses was measured. Black circles show the sum of counts in the overlapping pulse region with  $\sqrt{N_{\text{counts}}}$  uncertainty bars. Red line shows a least squares fit to a sinusoid. Inset shows the four output pulses (middle two overlapping) in the case of the maximally constructive (black dashed line) and maximally destructive (red line) interference.

$\bar{n} = 0.30$  and  $\bar{n} = 0.60$ . With these values, the decoy state method [17, 28, 30] was used to calculate a bound on the fidelity for storing single photon states  $F^{(n=1)} \geq 93.7\% \pm 2.4\%$ , which exceeds the classical limit of  $F = 2/3$ . Similar to the case for visibility discussed above, the measured fidelity was limited in part by dark counts and in part by the double comb protocol being an imperfect interferometer [17].

While the storage presented here was limited in efficiency, a nanophotonic cavity coupled to  $^{167}\text{Er}^{3+}$  ions in YSO promises to be an efficient quantum storage system. The main limitations to the storage efficiency in this work were a low ensemble cooperativity of 0.3 and loss from the optical nanobeam cavity. The cooperativity can be increased using higher  $^{167}\text{Er}^{3+}$  doping and better hyperfine initialization, which would require increasing the applied magnetic field or changing its angle [9, 17]. A higher intrinsic quality factor resonator would serve to both increase cooperativity and decrease cavity loss. For example, using a YSO crystal with 200 ppm  $^{167}\text{Er}^{3+}$  doping, optimal hyperfine initialization, and a resonator with an intrinsic quality factor of 2 million, the theoretical efficiency of the AFC quantum storage is 90% (see supplementary material for analysis [17]). Using a silicon resonator evanescently coupled to  $^{167}\text{Er}^{3+}$  ions in YSO [8, 31] would allow leveraging mature silicon nanofabrication technology to achieve this goal. With this efficiency level and a storage time of 10  $\mu\text{s}$ , the device would outperform standard telecommunications fiber [32], an important measure of success for optical quantum memories. With the optical AFC protocol alone, it may be difficult to achieve efficient storage for this duration due to the limit on narrowness of spectral features set by superhyperfine coupling. However, the AFC spin-wave protocol, where the stored information is reversibly transferred from the optical to the hyperfine manifold [12], would enable even longer storage without the same requirements for narrow spectral features, as well as adding on-demand recall capability. The availability of hyperfine states with coherence times exceeding 1 second [9] make  $^{167}\text{Er}^{3+}:\text{YSO}$  a promising system for spin-wave storage.

In conclusion, we have demonstrated on-chip quantum storage of telecommunications band light at the single photon level. The storage had a bandwidth of  $\sim 90$  MHz, and a storage fidelity for single photon states of at least  $93.7\% \pm 2.4\%$ .  $^{167}\text{Er}^{3+}:\text{YSO}$  at dilution refrigerator temperatures and moderate magnetic field was shown to be a promising material for AFC quantum memories. A clear path exists for creating a high efficiency quantum

memory using this material and a nanoscale resonator.

- 
- [1] H. J. Kimble, *Nature* **453**, 1023 (2008).
  - [2] K. Heshami, D. G. England, P. C. Humphreys, P. J. Bustard, V. M. Acosta, J. Nunn, and B. J. Sussman, *Journal of Modern Optics* **63**, 2005 (2016).
  - [3] H.-J. Briegel, W. Dür, J. I. Cirac, and P. Zoller, *Phys. Rev. Lett.* **81**, 5932 (1998).
  - [4] P. Kok, W. J. Munro, K. Nemoto, T. C. Ralph, J. P. Dowling, and G. J. Milburn, *Rev. Mod. Phys.* **79**, 135 (2007).
  - [5] C. Monroe, R. Raussendorf, A. Ruthven, K. R. Brown, P. Maunz, L.-M. Duan, and J. Kim, *Phys. Rev. A* **89**, 022317 (2014).
  - [6] C. Thiel, T. Böttger, and R. Cone, *Journal of Luminescence* **131**, 353 (2011).
  - [7] M. Zhong, M. P. Hedges, R. L. Ahlefeldt, J. G. Bartholomew, S. E. Beavan, S. M. Wittig, J. J. Longdell, and M. J. Sellars, *Nature* **517**, 177 (2015).
  - [8] E. Miyazono, I. Craiciu, A. Arbabi, T. Zhong, and A. Faraon, *Opt. Express* **25**, 2863 (2017).
  - [9] M. Rančić, M. P. Hedges, R. L. Ahlefeldt, and M. J. Sellars, *Nature Physics* **14**, 50 (2018).
  - [10] E. Saglamyurek, J. Jin, V. B. Verma, M. D. Shaw, F. Marsili, S. W. Nam, D. Oblak, and W. Tittel, *Nature Photonics* **9**, 83 (2015).
  - [11] M. F. Askarani, M. G. Pugibert, T. Lutz, V. B. Verma, M. D. Shaw, S. W. Nam, N. Sinclair, D. Oblak, and W. Tittel, (2018), arXiv:<https://arxiv.org/abs/1804.05699>.
  - [12] M. Afzelius, C. Simon, H. de Riedmatten, and N. Gisin, *Phys. Rev. A* **79**, 052329 (2009).
  - [13] M. Nilsson and S. Kröll, *Optics Communications* **247**, 393 (2005).
  - [14] B. Lauritzen, J. Minář, H. de Riedmatten, M. Afzelius, N. Sangouard, C. Simon, and N. Gisin, *Phys. Rev. Lett.* **104**, 080502 (2010).
  - [15] B. Lauritzen, J. Minář, H. de Riedmatten, M. Afzelius, and N. Gisin, *Phys. Rev. A* **83**, 012318 (2011).
  - [16] J. Dajczgewand, J.-L. L. Gouët, A. Louchet-Chauvet, and T. Chanelière, *Opt. Lett.* **39**, 2711 (2014).
  - [17] See Supplemental Material at **URL will be inserted by publisher** for material characterization details and calculation of storage cooperativity, fidelity, and efficiency.
  - [18] T. Zhong, J. Rochman, J. M. Kindem, E. Miyazono, and A. Faraon, *Opt. Express* **24**, 536

- (2016).
- [19] T. Zhong, J. M. Kindem, E. Miyazono, and A. Faraon, *Nature Communications* **6**, 8206 (2015).
- [20] T. Zhong, J. M. Kindem, J. G. Bartholomew, J. Rochman, I. Craiciu, E. Miyazono, M. Bettinelli, E. Cavalli, V. Verma, S. W. Nam, F. Marsili, M. D. Shaw, A. D. Beyer, and A. Faraon, *Science* (2017), 10.1126/science.aan5959.
- [21] S. Mosor, J. Hendrickson, B. C. Richards, J. Sweet, G. Khitrova, H. M. Gibbs, T. Yoshie, A. Scherer, O. B. Shchekin, and D. G. Deppe, *Applied Physics Letters* **87**, 141105 (2005).
- [22] I. Diniz, S. Portolan, R. Ferreira, J. M. Gérard, P. Bertet, and A. Auffèves, *Phys. Rev. A* **84**, 063810 (2011).
- [23] M. Afzelius and C. Simon, *Phys. Rev. A* **82**, 022310 (2010).
- [24] S. A. Moiseev, S. N. Andrianov, and F. F. Gubaidullin, *Phys. Rev. A* **82**, 022311 (2010).
- [25] H. de Riedmatten, M. Afzelius, M. U. Staudt, C. Simon, and N. Gisin, *Nature* **456**, 773 (2008).
- [26] O. Guillot-Noël, H. Vezin, P. Goldner, F. Beaudoux, J. Vincent, J. Lejay, and I. Lorgeré, *Phys. Rev. B* **76**, 180408 (2007).
- [27] B. Car, L. Veissier, A. Louchet-Chauvet, J.-L. Le Gouët, and T. Chanelière, *Phys. Rev. Lett.* **120**, 197401 (2018).
- [28] N. Sinclair, E. Saglamyurek, H. Mallahzadeh, J. A. Slater, M. George, R. Ricken, M. P. Hedges, D. Oblak, C. Simon, W. Sohler, and W. Tittel, *Phys. Rev. Lett.* **113**, 053603 (2014).
- [29] S. Welinski, C. W. Thiel, J. Dajczgewand, A. Ferrier, R. L. Cone, R. M. Macfarlane, T. Chanelière, A. Louchet-Chauvet, and P. Goldner, *Optical Materials* **63**, 69 (2017).
- [30] X. Ma, B. Qi, Y. Zhao, and H.-K. Lo, *Phys. Rev. A* **72**, 012326 (2005).
- [31] A. M. Dibos, M. Raha, C. M. Phenicie, and J. D. Thompson, *Phys. Rev. Lett.* **120**, 243601 (2018).
- [32] Y.-W. Cho, G. T. Campbell, J. L. Everett, J. Bernu, D. B. Higginbottom, M. T. Cao, J. Geng, N. P. Robins, P. K. Lam, and B. C. Buchler, *Optica* **3**, 100 (2016).

# Supplementary Materials for Technical Report

## Nanophotonic quantum storage at telecommunications wavelength

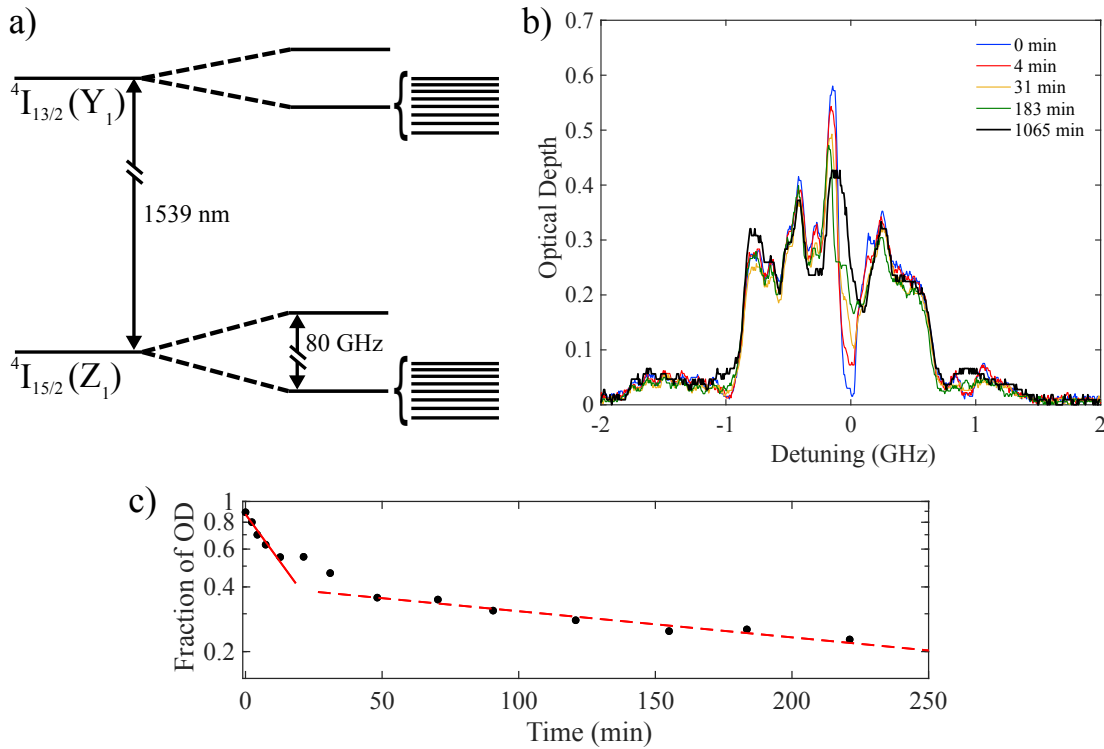
## I. EXPERIMENTAL DETAILS

A fiber-coupled tunable external-cavity diode laser was used to probe the nanobeam device and implement the AFC storage protocol. One percent of the laser light was directed to a wavemeter for measurement. Another one percent of the laser light was picked off and sent to a locking setup, in which the laser frequency was stabilized by locking to a home-built fiber cavity using the Pound-Drever-Hall technique [1]. The rest of the light was directed through two acousto-optical modulators (AOMs) for pulse shaping. An electro-optic phase modulator (EOM) was used to generate strong sidebands necessary for initialization (see Section III). The EOM was also used to add a  $\pi$  phase shift to pulses as required for fidelity measurements (see Section VII). Neutral density (ND) filters and polarization paddles provided attenuation and polarization control, respectively. A circulator directed light to the  $^{167}\text{Er}^{3+}:\text{YSO}$  crystal located inside a dilution refrigerator. The sample was mounted using indium solder onto a copper plate, which was thermally contacted to the 25 mK stage of a dilution refrigerator. A stack of  $xyz$  nanopositioners under the plate was used to optimize free space coupling. An aspheric lens pair focused light from a fiber onto the angled coupler of the resonator. Light from the sample was directed through the circulator onto a superconducting nanowire single photon detector (SNSPD) at  $\sim 100$  mK. A micro electro-mechanical switch prevented strong initialization and comb creation pulses from reaching the SNSPD. A magnetic field  $\mathbf{B} = 380$  mT was applied to the sample using two cylindrical permanent magnets for all measurements.

## II. SPECTRAL INITIALIZATION AND HYPERFINE $T_1$ IN BULK $^{167}\text{Er}^{3+}:\text{YSO}$

The hyperfine lifetime ( $T_1$ ) of  $^{167}\text{Er}^{3+}$  ions in YSO was measured using spectrally resolved optical pumping in an applied field of 380 mT parallel to the  $D_1$  crystal axis, and a nominal temperature of 25 mK. SM Figure 1a shows a schematic of the  $^{167}\text{Er}^{3+}:\text{YSO}$  energy levels. With a splitting of 80 GHz at 25 mK, the electron spin is frozen ( $\hbar\omega \ll k_B T$ ).

SM Figure 1b shows a scan of the inhomogeneously broadened  $^{167}\text{Er}^{3+}:\text{YSO}$  absorption line (black curve) in a bulk crystal. Transitions between individual hyperfine levels (in the lower electron spin branch) in the optical ground and excited state manifolds are partially resolved. A wide spectral transparency (trench) was created in this absorption line by



SM Figure 1. a) Schematic of energy levels of  $^{167}\text{Er}^{3+}:\text{YSO}$  with an applied field of 380 mT parallel to the  $D_1$  crystal axis. For crystallographic site 2, the  $^4I_{15/2} \rightarrow ^4I_{13/2}$  transition between the lowest crystal field levels corresponds to a wavelength of 1539 nm [2]. Each of these levels ( $Z_1$  and  $Y_1$ ) is an electron spin doublet that, which the applied magnetic field splits by 80 GHz [3]. The  $I = 7/2$  nuclear spin of  $^{167}\text{Er}^{3+}$  splits each electron spin level into 8. The bottom 8 levels of both the ground and excited manifolds are shown. These are the levels participating in the optical transitions studied in this work. b) Inhomogeneous  $^{167}\text{Er}^{3+}:\text{YSO}$  line showing the hyperfine structure and a spectral trench at 0 GHz detuning, shown as a function of time after trench creation. The detuning is measured from  $194814 \text{ GHz} \pm 1 \text{ GHz}$ . c) Depth of trench as a fraction of optical depth (OD) as a function of time after trench creation.

optical pumping: a laser was scanned slowly and repeatedly over a 140 MHz band, which depleted those hyperfine levels with resonant transitions. The population was then allowed to return to its equilibrium distribution while measuring transmission using a room temperature InGaAs photodiode. The last measured distribution among ground state hyperfine levels was not thermal, as the long relaxation times prevent timely thermalization and even scanning the inhomogeneous line redistributes population. Scanning the line to probe the hole depth

likely led to an underestimation of  $T_1$  by redistributing population, but this effect was minimized by using low scan power.

The width of the trench was chosen to minimize effects of spectral diffusion on the  $T_1$  measurement. The depth of the spectral feature, or hole depth  $d$ , is a measure of how much population was pumped away from the hyperfine levels that were optically addressed:

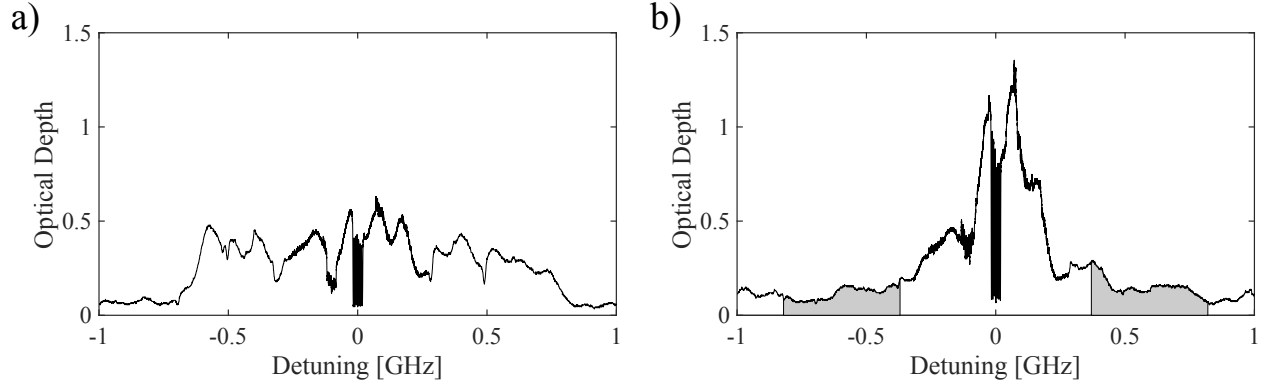
$$d(t) = \frac{\text{optical depth}(t \rightarrow \infty) - \text{optical depth}(t)}{\text{optical depth}(t \rightarrow \infty)}. \quad (1)$$

The maximum  $d(t)$  achieved here was 0.9. This was partly limited by the large trench width, which was likely spanning multiple hyperfine transitions, leading to some pumping of population as the laser is swept to create the trench. Using smaller trenches, holes with depth of  $\sim 0.93$  were measured, where it became difficult to accurately measure the depth of the hole due to a noisy background from detector noise and Fabry-Perot resonances in the setup. It is also possible that hole depth is limited by the  $^{167}\text{Er}^{3+}$  isotopic purity.

SM Figure 1c shows the decay in time of the hole depth  $d(t)$  as measured in the center of the trench. The fast decay is fit to an exponential with a lifetime of 29 min, while the slow decay is fit to a lifetime of 6 hours. Following Reference [4], we interpret these lifetimes as a two-step change in the spectrum: first the trench fills in due to spin-spin interactions between  $^{167}\text{Er}^{3+}$  ions, then, at a slower rate, the population is redistributed among hyperfine levels due to spin-lattice interactions.

### III. HYPERFINE INITIALIZATION – DISCUSSION AND BULK RESULTS

Due to the hyperfine splitting in both ground and excited state manifolds in  $^{167}\text{Er}^{3+}:\text{YSO}$ , the inhomogeneous linewidth is effectively broadened from its true value of  $\sim 150$  MHz to  $\sim 1.5$  GHz, decreasing the optical depth in the center of the line, relative to an isotope with zero nuclear spin. Moving population into fewer hyperfine states can increase this optical depth. At high magnetic fields, the entire optical ground state population can be initialized into one hyperfine state [4] by pumping on all  $\Delta m = +1$  or all  $\Delta m = -1$  transitions. At 380 mT  $\parallel D_1$ , only a partial initialization can be performed because the  $\Delta m = \pm 1$  transitions are not fully resolved from the  $\Delta m = 0$  transitions. SM Figure 2 shows the  $^{167}\text{Er}^{3+}:\text{YSO}$  1539 nm transition in a bulk crystal, both with and without initialization, always with a spectral comb created in the center. Initialization was performed by turning on strong sidebands of



SM Figure 2. Absorption spectrum of the inhomogeneous line in bulk  $^{167}\text{Er}^{3+}:\text{YSO}$  at 18 mK and 380 mT (parallel to  $D_1$ ) with 40 MHz wide comb created in the center. a) Without initialization, peak optical depth of comb is 0.4. b) With initialization into few hyperfine states before comb creation, peak optical depth of comb is 0.9. Grey area shows the extent of the sweep of the EOM sidebands during the initialization step. The detuning was measured from  $194814 \text{ GHz} \pm 1 \text{ GHz}$ .

the EOM modulator, and sweeping their detuning over a range of  $\pm(0.37 \text{ GHz} - 0.82 \text{ GHz})$ . This was the full range of the voltage controlled oscillator used to sweep the sidebands. A pulse sequence schematic is shown in Fig. 2b of the main text. This procedure moved population from the higher and lower energy hyperfine states to the middle few hyperfine states. The optical depth was improved by a factor of  $\sim 3$  compared to the uninitialized case, both in the bulk case shown in SM Fig. 2, and in the nanobeam, shown in the inset of Fig. 3c in the main text. Sweeping one sideband to pump on only one side of the inhomogeneous line produced a similar enhancement in optical depth. Preliminary studies have indicated that changing the angle of the magnetic field can also lead to separation of  $\Delta m = \pm 1$  transitions from the  $\Delta m = 0$  transitions for fields as low as 1 T, which would enable efficient hyperfine initialization at moderate magnetic fields.

#### IV. FITTING THE CAVITY REFLECTION CURVE TO EXTRACT ENSEMBLE COOPERATIVITY

To extract the cooperativity of the coupling between the nanobeam resonator and the ensemble of  $^{167}\text{Er}^{3+}$  ions, we fit each cavity reflection spectrum shown in the inset of Figure

1c in the main text to

$$R = \alpha_1 \left| (1 - \alpha_f) + \alpha_f e^{i\theta_f} - \frac{i\kappa_{\text{coupling}}}{\omega - \omega_{\text{cavity}} + i\frac{\kappa}{2} + W(\omega, g_{\text{total}}, \Delta_{\text{ions}}, \omega_{\text{ions}})} \right|^2 + \alpha_2. \quad (2)$$

where  $\alpha_{1,2}$  are amplitude and background fit parameters,  $\alpha_f e^{i\theta_f}$  accounts for Fano interference (both  $\alpha_f$  and  $\theta_f$  are fit parameters),  $\kappa$  is the total cavity energy decay rate,  $\kappa_{\text{coupling}}$  is the coupling rate through the input/output port, and  $\omega_{\text{cavity}}$  is the cavity resonance frequency.  $\kappa = 27.3$  and  $\frac{\kappa_{\text{coupling}}}{\kappa} = 0.21$  were measured from reflectivity curves where the cavity was detuned from the  $^{167}\text{Er}^{3+}$  transition.  $W(\omega, g_{\text{total}}, \Delta_{\text{ions}}, \omega_{\text{ions}})$  is the absorption rate of the cavity field by the ensemble of ions,  $W \sim \sum_i \frac{g_i^2}{\omega - \omega_i}$ , where  $g_i$  is the coupling between one ion and the cavity [5, 6]. We approximate the irregular inhomogeneous/hyperfine line as a Gaussian, and take from Reference [6] the expression for  $W$ :

$$W = i \frac{\sqrt{\pi \log 2} g_{\text{total}}^2}{\Delta_{\text{ions}}/2} \left[ 1 - \text{erfz} \left( -\frac{i\sqrt{\log 2}(\omega - \omega_{\text{ions}})}{\Delta_{\text{ions}}/2} \right) \right] \exp \left[ -\sqrt{\log 2} \left( \frac{\omega - \omega_{\text{ions}}}{\Delta_{\text{ions}}/2} \right)^2 \right], \quad (3)$$

where  $\Delta_{\text{ions}}$  is the linewidth of the ensemble transition,  $\omega_{\text{ions}}$  its the center,  $g_{\text{total}}^2 = \sum_i g_i^2$ . Finally, the ensemble cooperativity was computed using  $C = \frac{|W(\omega=\omega_{\text{ions}})|}{\kappa/2} = \frac{4\sqrt{\pi \log 2} g_{\text{total}}^2}{\kappa \Delta_{\text{ions}}}$  [7].

For the case with no initialization, the fit gave:  $\omega_{\text{cavity}} - \omega_{\text{ions}} = 2\pi \times 2.5$  GHz,  $g_{\text{total}} = 2\pi \times 0.79$  GHz,  $\Delta_{\text{ions}} = 2\pi \times 1.4$  GHz,  $C = 0.1$ .

For the case with initialization, the fit gave:  $\omega_{\text{cavity}} - \omega_{\text{ions}} = 2\pi \times 1.5$  GHz,  $g_{\text{total}} = 2\pi \times 0.70$  GHz,  $\Delta_{\text{ions}} = 2\pi \times 0.36$  GHz,  $C = 0.3$ .

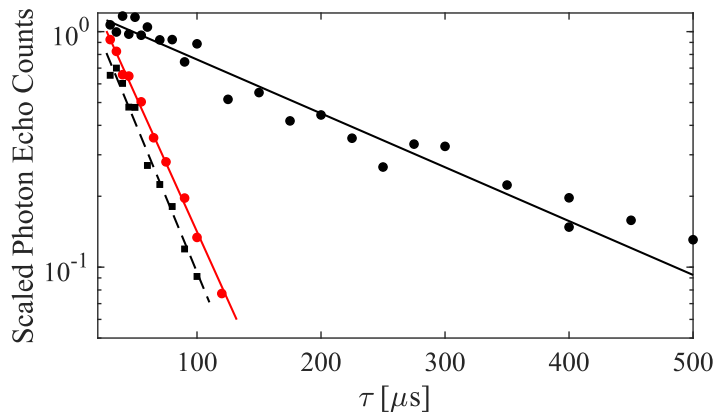
## V. COMPARISON OF THE OPTICAL $T_2$ TIME IN BULK AND IN THE NANOBEAM

By measuring two pulse photon echoes [8] as a function of time delay between pulses, the optical coherence time of ensembles of  $^{167}\text{Er}^{3+}$ :YSO ions was characterized in the center of the 1539 nm transition distribution, as shown in SM Figure 3. The laser was frequency stabilized by PDH locking to a home-built fiber cavity when measuring the bulk coherence at 35 mK ( $T_2 = 760 \mu\text{s}$ ). Without laser locking, this same curve had a double decay with a shorter exponential decay lifetime  $\sim 240 \mu\text{s}$ , which we interpret as being limited by laser frequency jitter. The coherence time of the ions coupled to the nanobeam cavity was  $\sim 1/4$  the coherence time of the bulk ions at the same temperature, but similar to the coherence time of the bulk ions at 1 K. It is likely that the measured coherence time of the ions coupled to the nanobeam is limited by heating due to the input pulse pairs, as the nanobeam has

poor thermal contact to the rest of the bulk crystal (through  $\sim 1 \mu\text{m}^2$  connections at either end). It was not possible to accurately simulate the device temperature during measurement due to lack of data on the low temperature thermal coefficient of YSO. It is also possible that the fabrication of the nanobeam resonator caused disorder that affected the coherence time of the ions. Rare-earth ions coupled to similar nanobeam resonators have been shown to have coherence times similar to the bulk [9, 10], however, the longer bulk coherence times measured in the current work allow a much more sensitive probe of the ions' environment.

## VI. ACCUMULATED VERSUS STEP-AND-PUMP ATOMIC FREQUENCY COMBS

Two different procedures were used to create the AFCs. For longer memory times, the frequency difference between the teeth of the comb must be smaller, so the teeth themselves need also be narrower. Laser frequency jitter limits the minimum width of comb teeth, so longer storage times necessitate frequency stabilization of the laser. With the step-and-pump method, the laser must be stepped in frequency, and the method used to lock the



SM Figure 3. Two pulse photon echo amplitudes versus inter-pulse time delay with exponential fits; the vertical axis is scaled for clarity.  $T_2$  was measured to be  $4 \times \tau(1/e) = 759 \mu\text{s} \pm 41 \mu\text{s}$  in bulk at 35 mK (black circles and solid black line fit),  $136 \mu\text{s} \pm 9 \mu\text{s}$  in bulk at 940 mK (black squares and dashed black line fit), and  $149 \mu\text{s} \pm 4 \mu\text{s}$  in the nanobeam at 42 mK (red circles and solid red line fit). All temperatures were measured at the dilution refrigerator stage to which the sample was thermally connected.

laser (feeding back to the current) did not allow for both stepping and stabilizing the laser frequency. With the accumulated AFC method, no frequency modulation is required, so frequency stabilization was possible, enabling longer memory times. However, for short memory times, where laser jitter did not adversely affect the width of the teeth, the step-and-pump method led to a higher efficiency because the depth of the teeth across the comb was homogeneous (with accumulated AFC, the frequency comb has a sinc function envelope).

## VII. FIDELITY MEASUREMENT

In the absence of a single photon source, a lower bound on the storage fidelity of a single photon input state can be found using the decoy state analysis method [11, 12]. In this method, a time bin state  $\psi$  with a mean photon number  $\bar{n}$  is stored using the AFC protocol, and the fidelity  $F_\psi^{(\bar{n})}$  of storage is measured as

$$F_\psi^{(\bar{n})} = \frac{N_\psi}{N_\psi + N_{\phi \perp \psi}}, \quad (4)$$

where  $N_i (i = \psi, \phi)$  is the number of photons measured in the output time bin corresponding to  $\psi$ , and  $\phi \perp \psi$  denotes the state orthogonal to  $\psi$ . The gain of the output,  $Q_\psi^{(\bar{n})}$  is also estimated using,

$$Q_\psi^{(\bar{n})} = N_\psi + N_{\phi \perp \psi}. \quad (5)$$

$F_\psi^{(\bar{n})}$  and  $Q_\psi^{(\bar{n})}$  are measured for mean photon numbers  $\bar{n}_1$  and  $\bar{n}_2$ , where  $\bar{n}_1 < \bar{n}_2$ , and  $\bar{n}_2 < 1$ . The lower bound on the fidelity of storing a one-photon input state  $F_\psi^{(n=1,L)}$  is then computed using:

$$F_\psi^{(n=1,L)} = 1 - \frac{E_\psi^{(\bar{n}_1)} Q^{(\bar{n}_1)} \exp \bar{n}_1 - E^{(n=0)} Y^{(n=0)}}{Y^{(n=1,L)} \bar{n}_1}, \quad (6)$$

where

$$E_\psi^{(\bar{n})} = 1 - F_\psi^{(\bar{n})} \quad (7)$$

is the error rate of storing a state  $\psi$  with mean photon number  $\bar{n}$ , and

$$Y^{(n=1,L)} = \max \left[ Y^{(n=0)}, \frac{\bar{n}_2}{\bar{n}_2 \bar{n}_1 - \bar{n}_1^2} \left( Q^{(\bar{n}_1)} \exp \bar{n}_1 - Q^{(\bar{n}_2)} \exp \bar{n}_2 \frac{\bar{n}_1^2}{\bar{n}_2^2} - \frac{\bar{n}_2^2 - \bar{n}_1^2}{\bar{n}_2^2} Y^{(n=0)} \right) \right] \quad (8)$$

is the lower bound on the detection yield for the storage of a single photon state (see Reference [11]).  $Y^{(n=0)} = Q^{(n=0)}$  is the yield when the input state is vacuum, equal to the dark counts in all output time bins. The superscripts denote photon number, and whether

the value is a lower bound ( $L$ ).  $E^{(n=0)}$  is the vacuum error rate, which is 0.5 by definition [11].

In order to obtain an average fidelity for all time bin states, the fidelities for storing time bin states  $|\text{early}\rangle$ ,  $|\text{late}\rangle$ ,  $|+\rangle = \frac{|\text{early}\rangle+|\text{late}\rangle}{\sqrt{2}}$  and  $|-\rangle = \frac{|\text{early}\rangle-|\text{late}\rangle}{\sqrt{2}}$  were measured for input photon numbers  $\bar{n} = 0.30$  and  $\bar{n} = 0.60$ . For input states  $|+\rangle$  and  $|-\rangle$ , an interferometer is required to measure  $N_\psi$  and  $N_{\phi\perp\psi}$ . Following Reference [13], a double atomic frequency comb was used as the interferometer, allowing for direct readout of  $F_+$  and  $F_-$ . The input pulses defining the  $|\text{early}\rangle$  and  $|\text{late}\rangle$  basis were 60 ns wide and 90 ns apart. A double AFC was used for measurements of all states, with the memory times associated with the two combs being  $t_1 = 210$  ns and  $t_2 = 300$  ns, such that  $t_1 - t_2 = 90$  ns. As SM Figure 4 shows, of the three output time bins, the first and third were used for measuring  $F_{\text{early}}$  and  $F_{\text{late}}$  while the second time bin was used for measuring  $F_+$  and  $F_-$ .

For computing the bound on the yield of a single photon in Equation 8,  $Q_-(Q_{\text{early}})$  and  $Q_+(Q_{\text{late}})$  were averaged to give  $Q_{+/-}$  ( $Q_{\text{early/late}}$ ), and the dark counts were averaged to give  $Y_{+/-}^{(n=0)}$  ( $Y_{\text{early/late}}^{(n=0)}$ ). From these, two different lower bounds on the single photon yield,  $Y_{+/-}^{(n=1,L)}$  and  $Y_{\text{early/late}}^{(n=1,L)}$  were computed. This was required because while the experiments to measure  $F_+$  and  $F_-$  were identical in every way except the input state, and the same holds for the experiments to measure  $F_{\text{early}}$  and  $F_{\text{late}}$ , the pairs of experiments differed from one another. For instance, because two output pulses overlapped to give a signal in measurements of  $F_+$  and  $F_-$ , the signal level was twice as large as for  $F_{\text{early}}$  and  $F_{\text{late}}$ , so the latter two experiments were conducted for twice as long to compensate.

Following Equation 6,  $F_+^{(n=1,L)}$  was therefore computed using:

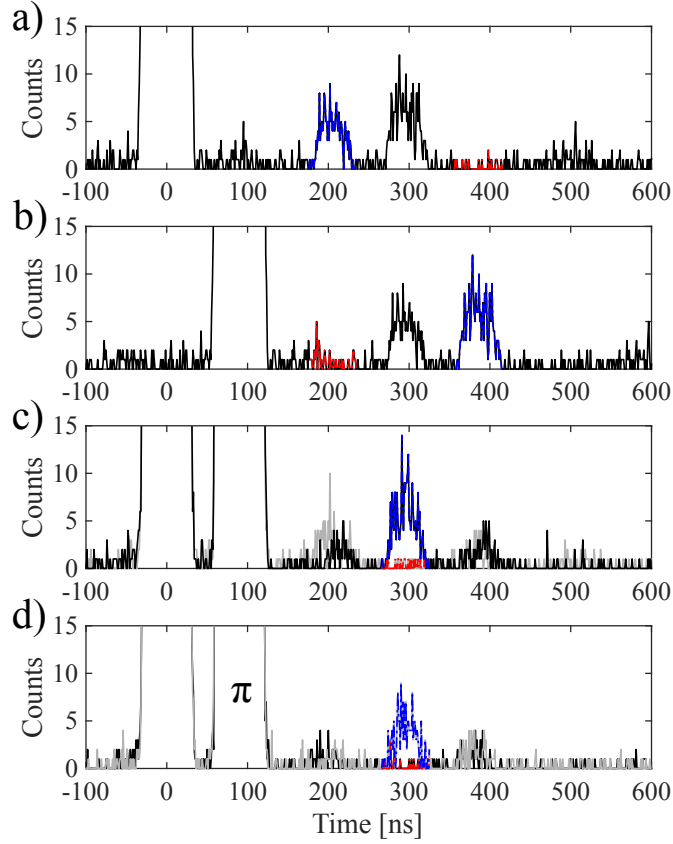
$$F_+^{(n=1,L)} = 1 - \frac{E_+^{(\bar{n}_1)} Q_{+/-}^{(\bar{n}_1)} \exp \bar{n}_1 - E^{(n=0)} Y_{+/-}^{(n=0)}}{Y_{+/-}^{(n=1,L)} \bar{n}_1}, \quad (9)$$

with similar equations for the other three states.

The lower bound on the fidelity of storing an arbitrary single photon state was then computed as follows:

$$F_{\text{average}}^{(n=1,L)} = \frac{1}{3} \left( \frac{F_{\text{early}}^{(n=1,L)} + F_{\text{late}}^{(n=1,L)}}{2} \right) + \frac{2}{3} \left( \frac{F_+^{(n=1,L)} + F_-^{(n=1,L)}}{2} \right). \quad (10)$$

Table I summarizes the fidelity data used to compute  $F_{\text{average}}^{(n=1,L)} = 93.7\% \pm 2.4\%$ . The



SM Figure 4. Part of the raw data used in the fidelity measurement.  $\bar{n} = 0.6$  input (left, cut off) and output pulses from double comb. Input pulses are time bin states a) early b) late, c) +, d) -. In all figures, blue (red) dash-dot line represents the 60 ns time bins counted as  $N_\psi$  ( $N_{\phi \perp \psi}$ ). Time resolution is 1 ns. The same data set, shown in a) and b), was used for both the early and late fidelity calculations, since absolute time is irrelevant. In this data set, a small pulse 100 ns after the read pulse can be seen. The origin of this pulse was unclear, but it disappeared in the absence of the double comb. In c) and d), the black curve represents data taken with comb detunings  $\delta_1 = \delta_2 = 0$ , while the grey curve represents data taken with  $\delta_1 = 0$ ,  $\delta_2 = \frac{\Delta_2}{2}$  ( $\phi_{\text{rel}} = \pi$ ).

uncertainties are calculated based on  $\sqrt{N_{\text{photon}}}$  standard deviation on all  $N_\psi$  values due to Poissonian statistics of photon counting and the uncertainty, estimated to be 15%, of the mean input photon numbers,  $\bar{n}$ .

There were two main limits to the measured fidelity. The first was dark counts, which are uniformly distributed SNSPD detection events with an average rate of 18 Hz, believed to be

Input photon number	$\frac{1}{2} (F_{\text{early}} + F_{\text{late}})$	$\frac{1}{2} (F_+ + F_-)$
$\bar{n} = 0.60 \pm 0.09$	$89.04\% \pm 1.34\%$	$91.90\% \pm 1.32\%$
$\bar{n} = 0.30 \pm 0.05$	$82.59\% \pm 1.80\%$	$90.75\% \pm 1.84\%$
$n = 0$	50%	50%
	$\frac{1}{2} (F_{\text{early}}^{(n=1,L)} + F_{\text{late}}^{(n=1,L)})$	$\frac{1}{2} (F_+^{(n=1,L)} + F_-^{(n=1,L)})$
$n = 1$	$89.85\% \pm 1.97\%$	$95.59\% \pm 3.37\%$

TABLE I. Measured fidelities of storage in the nanobeam device.

caused by environmental photons at a wide range of wavelengths and electronic noise. The dark counts limited fidelity bound was estimated to be  $\sim 96.5\%$ . The remaining reduction in measured fidelity was caused by the double AFC being an imperfect interferometer. Specifically, we observed: (i) imperfect cancellation of the overlapped output pulses in the case of destructive interference, resulting from the different efficiencies of output pulses generated by the two spectral combs; (ii) a peak found at  $\sim 100$  ns that is an unexpected result of the double comb procedure, shown in SM Fig. 4b.

### VIII. PREDICTED EFFICIENCY OF AFC STORAGE: CURRENT DEVICE AND FUTURE IMPROVEMENT

As described in References [5, 10, 14], the efficiency of an AFC memory in a resonator is given by:

$$\eta_{AFC} = \left( \frac{4\kappa_{\text{coupling}} \Gamma_{\text{comb}}}{(\kappa_{\text{total}} + \Gamma_{\text{comb}} + \Gamma_{\text{bg}})^2} \right)^2 \exp \left( -\frac{\pi^2}{2 \ln 2 (\Delta/\gamma)^2} \right). \quad (11)$$

The effective cooperativity  $C'$  of the atomic frequency comb is defined as:

$$C' \equiv \frac{\Gamma_{\text{comb}} + \Gamma_{\text{bg}}}{\kappa_{\text{total}}/2}, \quad (12)$$

where  $\Gamma_{\text{comb}}$  and  $\Gamma_{\text{bg}}$  are the absorption rates of the cavity field by the ensemble of ions in the comb and background, respectively. The background ions are the ions remaining after optical pumping, with transition frequencies where transparency is desired (i.e. between the teeth of the comb). Nonzero  $\Gamma_{\text{bg}}$  results from limitations in spectral holeburning, as discussed in Section II. Using  $\eta_{\text{spectral}}$ , the fractional optical depth of a spectral hole (in the language of Section II,  $\eta_{\text{spectral}} = d(t=0)$ ),  $\Delta$ , the inter-tooth spacing, and  $\gamma$ , the width of

one comb tooth, these can be estimated as follows:

$$\Gamma_{\text{comb}} \approx \eta_{\text{spectral}} \frac{\gamma}{\Delta} \Gamma_{\text{ions}}, \quad (13)$$

$$\Gamma_{\text{bg}} = (1 - \eta_{\text{spectral}}) \Gamma_{\text{ions}}, \quad (14)$$

where

$$\begin{aligned} \eta_{\text{spectral}} &= \frac{N_{\text{ions}}(\text{comb peak}) - N_{\text{ions}}(\text{comb trough})}{N_{\text{ions}}(\text{comb peak})} \\ &= \frac{\text{initial optical depth} - \text{optical depth post initialization}}{\text{initial optical depth}} \end{aligned}$$

and  $\Gamma_{\text{ions}} = |W(\omega = \omega_{\text{ions}})| = \frac{\sqrt{\pi \log 2} g_{\text{total}}^2}{\Delta_{\text{ions}}/2}$  is the absorption rate of the cavity field by the ensemble of ions before comb preparation (see Section IV). The effective cooperativity  $C'$  is therefore related to the cooperativity before the comb was created,  $C$  by  $C' = (\eta_{\text{spectral}} \frac{\gamma}{\Delta} + (1 - \eta_{\text{spectral}}))C$ . Rewriting the equation gives rise to the following expression for the memory efficiency of a real comb:

$$\eta_{\text{AFC}} = \left( \frac{1}{\frac{\Delta}{\gamma} \left( \frac{1}{\eta_{\text{spectral}}} - 1 \right) + 1} \frac{\kappa_{\text{coupling}}}{\kappa_{\text{total}}} \frac{4C'}{(1 + C')^2} \right)^2 \exp \left( -\frac{\pi^2}{2 \ln 2 (\Delta/\gamma)^2} \right). \quad (15)$$

The predicted efficiency for this device is  $\eta_{\text{AFC}} = 0.17\%$ , found using  $C = 0.3$ ,  $\frac{\kappa_{\text{coupling}}}{\kappa_{\text{total}}} = 0.21$ , a measured fidelity of  $\Delta/\gamma = 2.1$ , and by assuming a perfect comb  $\eta_{\text{spectral}} = 1$  (giving  $C' = 0.14$ ). This is similar to the measured value of  $0.20\%$  for a storage time of 165 ns.

To improve the memory efficiency, the two most important improvements that can be made are to increase the ensemble cooperativity, and to improve the ratio  $\frac{\kappa_{\text{coupling}}}{\kappa_{\text{total}}}$ . The first of these can be accomplished by increasing the doping of erbium in the YSO crystal ( $\times 4$  increase in  $C$  by increasing the ion concentration to 200 ppm, assuming no significant increase in inhomogeneous linewidth), and also by initializing into a single hyperfine state with 95% efficiency [4], before preparing a comb (an expected increase in  $C$  of approximately  $\times 2.5$ ). Using  $C = 3$  and  $\frac{\kappa_{\text{coupling}}}{\kappa_{\text{total}}} = 0.21$ , and a comb finesse of  $\Delta/\gamma = 3$ , ( $C' = 0.73$ ), the predicted efficiency is 3%.

At this point, the memory efficiency is mainly limited by the loss from the cavity. In the case of perfectly narrow, perfectly absorbing comb teeth with no background,  $C' \rightarrow 1$ ,  $\Delta/\gamma \rightarrow \infty$ ,  $\eta_{\text{spectral}} \rightarrow 1$ , the efficiency of the AFC becomes  $\left( \frac{\kappa_{\text{coupling}}}{\kappa_{\text{total}}} \right)^2 = \left( 1 - \frac{\kappa_{\text{intrinsic}} + \kappa_{\text{mirror 2}}}{\kappa_{\text{total}}} \right)^2$ . That is, in the limit of perfect spectral tailoring, the memory efficiency is limited by what fraction of the cavity decay rate is through the coupling port.

A memory efficiency greater than 90% can be achieved if the intrinsic quality factor of the resonator is increased from its current value of  $Q_i \sim 9000$  to 2 million, while increasing  $\frac{\kappa_{\text{coupling}}}{\kappa_{\text{total}}}$  to 0.97. The latter can be accomplished by making a resonator with one mirror having a relatively lower reflectivity, and with minimal losses through other channels (transmission through second mirror, scattering, absorption). This calculation assumes the same material as described above (200 ppm, ideal initialization into one hyperfine state), and a comb finesse of  $\sim 13$ . It also accounts for a decrease by a factor of  $\sim 3$  in the cooperativity that results from switching to a hybrid silicon-YSO platform where the cavity-ion coupling is decreased because the optical mode couples evanescently to the ions. At this efficiency, the memory would match the performance of an optical fiber (0.15 dB/km) at  $t_{\text{storage}} = 10 \mu\text{s}$  [15].

For a finesse of 13 and a storage time of  $10 \mu\text{s}$ , the corresponding comb tooth width is  $\gamma = \frac{\Delta}{\text{finesse}} = 8 \text{ kHz}$ . This is too narrow for a material doped with Kramer's ions such as  $^{167}\text{Er}^{3+}:\text{YSO}$ , where effective linewidths are limited by superhyperfine coupling to the host material's nuclear spins. In  $\text{Er}^{3+}:\text{YSO}$ , superhyperfine broadening is of the order of 1 MHz [16, 17]. However, long memory times can still be achieved with a nanoresonator in this material by using the spin-wave AFC, where the stored coherence is transferred from the optical to the hyperfine manifold and back [18]. Coherence times of greater than 1 second have been measured for the hyperfine levels in  $^{167}\text{Er}^{3+}:\text{YSO}$  [4].

- 
- [1] R. W. P. Drever, J. L. Hall, F. V. Kowalski, J. Hough, G. M. Ford, A. J. Munley, and H. Ward, *Appl. Phys. B* **31**, 97 (1983).
  - [2] T. Böttger, Y. Sun, C. W. Thiel, and R. L. Cone, *Phys. Rev. B* **74**, 075107 (2006).
  - [3] Y. Sun, T. Böttger, C. W. Thiel, and R. L. Cone, *Phys. Rev. B* **77**, 085124 (2008).
  - [4] M. Rančić, M. P. Hedges, R. L. Ahlefeldt, and M. J. Sellars, *Nature Physics* **14**, 50 (2018).
  - [5] M. Afzelius and C. Simon, *Phys. Rev. A* **82**, 022310 (2010).
  - [6] I. Diniz, S. Portolan, R. Ferreira, J. M. Gérard, P. Bertet, and A. Auffèves, *Phys. Rev. A* **84**, 063810 (2011).
  - [7] E. Miyazono, I. Craiciu, A. Arbabi, T. Zhong, and A. Faraon, *Opt. Express* **25**, 2863 (2017).
  - [8] I. D. Abella, N. A. Kurnit, and S. R. Hartmann, *Phys. Rev.* **141**, 391 (1966).
  - [9] T. Zhong, J. M. Kindem, E. Miyazono, and A. Faraon, *Nature Communications* **6**, 8206

- (2015).
- [10] T. Zhong, J. M. Kindem, J. G. Bartholomew, J. Rochman, I. Craiciu, E. Miyazono, M. Bettinelli, E. Cavalli, V. Verma, S. W. Nam, F. Marsili, M. D. Shaw, A. D. Beyer, and A. Faraon, *Science* (2017), 10.1126/science.aan5959.
  - [11] X. Ma, B. Qi, Y. Zhao, and H.-K. Lo, *Phys. Rev. A* **72**, 012326 (2005).
  - [12] N. Sinclair, E. Saglamyurek, H. Mallahzadeh, J. A. Slater, M. George, R. Ricken, M. P. Hedges, D. Oblak, C. Simon, W. Sohler, and W. Tittel, *Phys. Rev. Lett.* **113**, 053603 (2014).
  - [13] H. de Riedmatten, M. Afzelius, M. U. Staudt, C. Simon, and N. Gisin, *Nature* **456**, 773 (2008).
  - [14] S. A. Moiseev, S. N. Andrianov, and F. F. Gubaidullin, *Phys. Rev. A* **82**, 022311 (2010).
  - [15] Y.-W. Cho, G. T. Campbell, J. L. Everett, J. Bernu, D. B. Higginbottom, M. T. Cao, J. Geng, N. P. Robins, P. K. Lam, and B. C. Buchler, *Optica* **3**, 100 (2016).
  - [16] O. Guillot-Noël, H. Vezin, P. Goldner, F. Beaudoux, J. Vincent, J. Lejay, and I. Lorgeré, *Phys. Rev. B* **76**, 180408 (2007).
  - [17] B. Car, L. Veissier, A. Louchet-Chauvet, J.-L. Le Gouët, and T. Chanelière, *Phys. Rev. Lett.* **120**, 197401 (2018).
  - [18] M. Afzelius, C. Simon, H. de Riedmatten, and N. Gisin, *Phys. Rev. A* **79**, 052329 (2009).

# Supplementary Materials for Technical Report

## Nanophotonic quantum storage at telecommunications wavelength

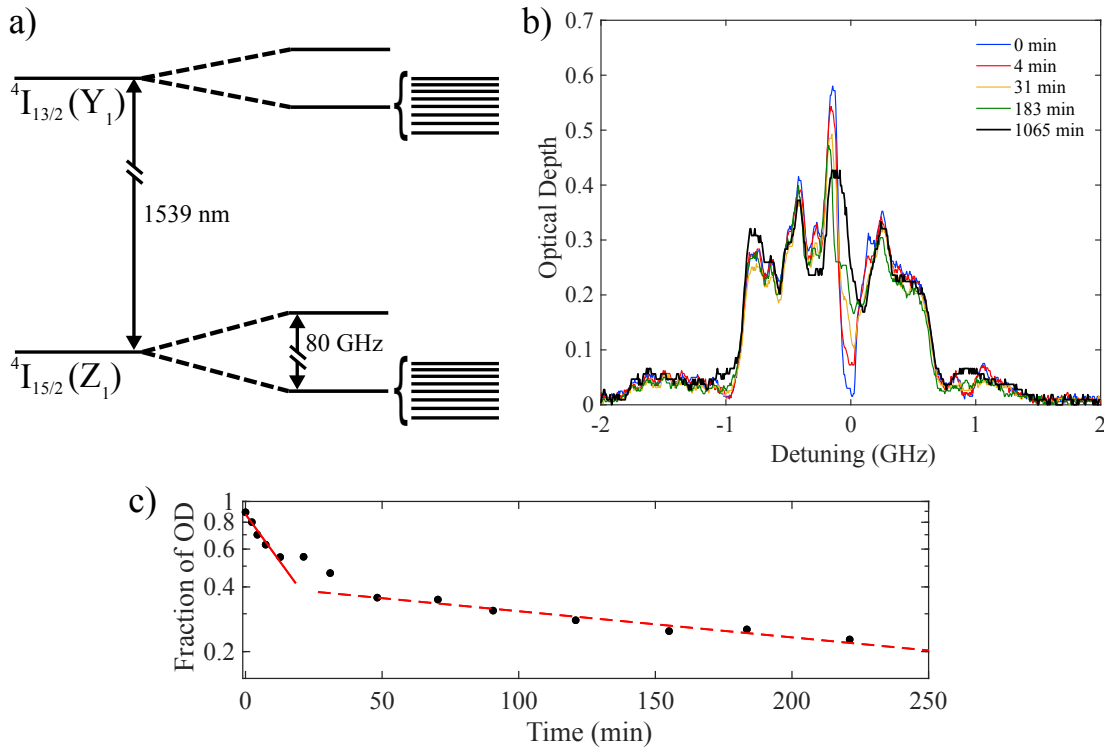
## I. EXPERIMENTAL DETAILS

A fiber-coupled tunable external-cavity diode laser was used to probe the nanobeam device and implement the AFC storage protocol. One percent of the laser light was directed to a wavemeter for measurement. Another one percent of the laser light was picked off and sent to a locking setup, in which the laser frequency was stabilized by locking to a home-built fiber cavity using the Pound-Drever-Hall technique [1]. The rest of the light was directed through two acousto-optical modulators (AOMs) for pulse shaping. An electro-optic phase modulator (EOM) was used to generate strong sidebands necessary for initialization (see Section III). The EOM was also used to add a  $\pi$  phase shift to pulses as required for fidelity measurements (see Section VII). Neutral density (ND) filters and polarization paddles provided attenuation and polarization control, respectively. A circulator directed light to the  $^{167}\text{Er}^{3+}:\text{YSO}$  crystal located inside a dilution refrigerator. The sample was mounted using indium solder onto a copper plate, which was thermally contacted to the 25 mK stage of a dilution refrigerator. A stack of  $xyz$  nanopositioners under the plate was used to optimize free space coupling. An aspheric lens pair focused light from a fiber onto the angled coupler of the resonator. Light from the sample was directed through the circulator onto a superconducting nanowire single photon detector (SNSPD) at  $\sim 100$  mK. A micro electro-mechanical switch prevented strong initialization and comb creation pulses from reaching the SNSPD. A magnetic field  $\mathbf{B} = 380$  mT was applied to the sample using two cylindrical permanent magnets for all measurements.

## II. SPECTRAL INITIALIZATION AND HYPERFINE $T_1$ IN BULK $^{167}\text{Er}^{3+}:\text{YSO}$

The hyperfine lifetime ( $T_1$ ) of  $^{167}\text{Er}^{3+}$  ions in YSO was measured using spectrally resolved optical pumping in an applied field of 380 mT parallel to the  $D_1$  crystal axis, and a nominal temperature of 25 mK. SM Figure 1a shows a schematic of the  $^{167}\text{Er}^{3+}:\text{YSO}$  energy levels. With a splitting of 80 GHz at 25 mK, the electron spin is frozen ( $\hbar\omega \ll k_B T$ ).

SM Figure 1b shows a scan of the inhomogeneously broadened  $^{167}\text{Er}^{3+}:\text{YSO}$  absorption line (black curve) in a bulk crystal. Transitions between individual hyperfine levels (in the lower electron spin branch) in the optical ground and excited state manifolds are partially resolved. A wide spectral transparency (trench) was created in this absorption line by



SM Figure 1. a) Schematic of energy levels of  $^{167}\text{Er}^{3+}:\text{YSO}$  with an applied field of 380 mT parallel to the  $D_1$  crystal axis. For crystallographic site 2, the  $^4I_{15/2} \rightarrow ^4I_{13/2}$  transition between the lowest crystal field levels corresponds to a wavelength of 1539 nm [2]. Each of these levels ( $Z_1$  and  $Y_1$ ) is an electron spin doublet that, which the applied magnetic field splits by 80 GHz [3]. The  $I = 7/2$  nuclear spin of  $^{167}\text{Er}^{3+}$  splits each electron spin level into 8. The bottom 8 levels of both the ground and excited manifolds are shown. These are the levels participating in the optical transitions studied in this work. b) Inhomogeneous  $^{167}\text{Er}^{3+}:\text{YSO}$  line showing the hyperfine structure and a spectral trench at 0 GHz detuning, shown as a function of time after trench creation. The detuning is measured from  $194814 \text{ GHz} \pm 1 \text{ GHz}$ . c) Depth of trench as a fraction of optical depth (OD) as a function of time after trench creation.

optical pumping: a laser was scanned slowly and repeatedly over a 140 MHz band, which depleted those hyperfine levels with resonant transitions. The population was then allowed to return to its equilibrium distribution while measuring transmission using a room temperature InGaAs photodiode. The last measured distribution among ground state hyperfine levels was not thermal, as the long relaxation times prevent timely thermalization and even scanning the inhomogeneous line redistributes population. Scanning the line to probe the hole depth

likely led to an underestimation of  $T_1$  by redistributing population, but this effect was minimized by using low scan power.

The width of the trench was chosen to minimize effects of spectral diffusion on the  $T_1$  measurement. The depth of the spectral feature, or hole depth  $d$ , is a measure of how much population was pumped away from the hyperfine levels that were optically addressed:

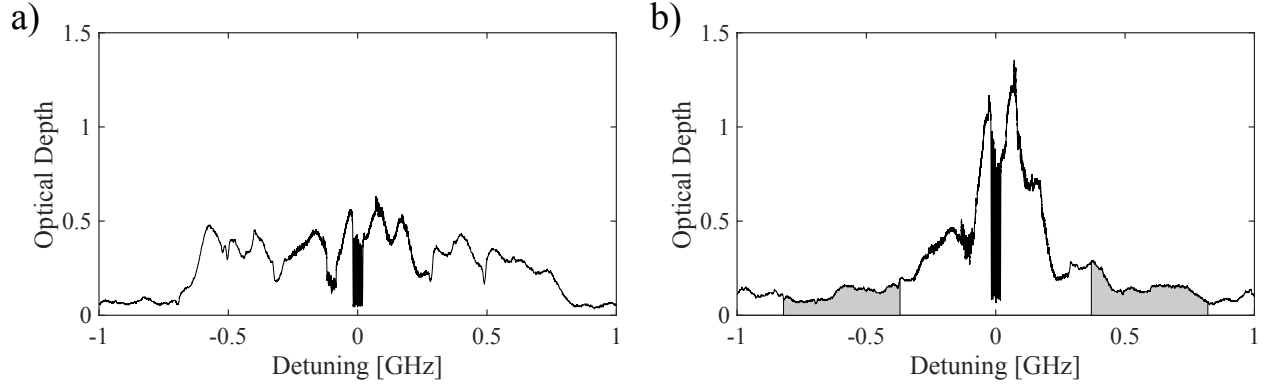
$$d(t) = \frac{\text{optical depth}(t \rightarrow \infty) - \text{optical depth}(t)}{\text{optical depth}(t \rightarrow \infty)}. \quad (1)$$

The maximum  $d(t)$  achieved here was 0.9. This was partly limited by the large trench width, which was likely spanning multiple hyperfine transitions, leading to some pumping of population as the laser is swept to create the trench. Using smaller trenches, holes with depth of  $\sim 0.93$  were measured, where it became difficult to accurately measure the depth of the hole due to a noisy background from detector noise and Fabry-Perot resonances in the setup. It is also possible that hole depth is limited by the  $^{167}\text{Er}^{3+}$  isotopic purity.

SM Figure 1c shows the decay in time of the hole depth  $d(t)$  as measured in the center of the trench. The fast decay is fit to an exponential with a lifetime of 29 min, while the slow decay is fit to a lifetime of 6 hours. Following Reference [4], we interpret these lifetimes as a two-step change in the spectrum: first the trench fills in due to spin-spin interactions between  $^{167}\text{Er}^{3+}$  ions, then, at a slower rate, the population is redistributed among hyperfine levels due to spin-lattice interactions.

### III. HYPERFINE INITIALIZATION – DISCUSSION AND BULK RESULTS

Due to the hyperfine splitting in both ground and excited state manifolds in  $^{167}\text{Er}^{3+}:\text{YSO}$ , the inhomogeneous linewidth is effectively broadened from its true value of  $\sim 150$  MHz to  $\sim 1.5$  GHz, decreasing the optical depth in the center of the line, relative to an isotope with zero nuclear spin. Moving population into fewer hyperfine states can increase this optical depth. At high magnetic fields, the entire optical ground state population can be initialized into one hyperfine state [4] by pumping on all  $\Delta m = +1$  or all  $\Delta m = -1$  transitions. At 380 mT  $\parallel D_1$ , only a partial initialization can be performed because the  $\Delta m = \pm 1$  transitions are not fully resolved from the  $\Delta m = 0$  transitions. SM Figure 2 shows the  $^{167}\text{Er}^{3+}:\text{YSO}$  1539 nm transition in a bulk crystal, both with and without initialization, always with a spectral comb created in the center. Initialization was performed by turning on strong sidebands of



SM Figure 2. Absorption spectrum of the inhomogeneous line in bulk  $^{167}\text{Er}^{3+}:\text{YSO}$  at 18 mK and 380 mT (parallel to  $D_1$ ) with 40 MHz wide comb created in the center. a) Without initialization, peak optical depth of comb is 0.4. b) With initialization into few hyperfine states before comb creation, peak optical depth of comb is 0.9. Grey area shows the extent of the sweep of the EOM sidebands during the initialization step. The detuning was measured from  $194814 \text{ GHz} \pm 1 \text{ GHz}$ .

the EOM modulator, and sweeping their detuning over a range of  $\pm(0.37 \text{ GHz} - 0.82 \text{ GHz})$ . This was the full range of the voltage controlled oscillator used to sweep the sidebands. A pulse sequence schematic is shown in Fig. 2b of the main text. This procedure moved population from the higher and lower energy hyperfine states to the middle few hyperfine states. The optical depth was improved by a factor of  $\sim 3$  compared to the uninitialized case, both in the bulk case shown in SM Fig. 2, and in the nanobeam, shown in the inset of Fig. 3c in the main text. Sweeping one sideband to pump on only one side of the inhomogeneous line produced a similar enhancement in optical depth. Preliminary studies have indicated that changing the angle of the magnetic field can also lead to separation of  $\Delta m = \pm 1$  transitions from the  $\Delta m = 0$  transitions for fields as low as 1 T, which would enable efficient hyperfine initialization at moderate magnetic fields.

#### IV. FITTING THE CAVITY REFLECTION CURVE TO EXTRACT ENSEMBLE COOPERATIVITY

To extract the cooperativity of the coupling between the nanobeam resonator and the ensemble of  $^{167}\text{Er}^{3+}$  ions, we fit each cavity reflection spectrum shown in the inset of Figure

1c in the main text to

$$R = \alpha_1 \left| (1 - \alpha_f) + \alpha_f e^{i\theta_f} - \frac{i\kappa_{\text{coupling}}}{\omega - \omega_{\text{cavity}} + i\frac{\kappa}{2} + W(\omega, g_{\text{total}}, \Delta_{\text{ions}}, \omega_{\text{ions}})} \right|^2 + \alpha_2. \quad (2)$$

where  $\alpha_{1,2}$  are amplitude and background fit parameters,  $\alpha_f e^{i\theta_f}$  accounts for Fano interference (both  $\alpha_f$  and  $\theta_f$  are fit parameters),  $\kappa$  is the total cavity energy decay rate,  $\kappa_{\text{coupling}}$  is the coupling rate through the input/output port, and  $\omega_{\text{cavity}}$  is the cavity resonance frequency.  $\kappa = 27.3$  and  $\frac{\kappa_{\text{coupling}}}{\kappa} = 0.21$  were measured from reflectivity curves where the cavity was detuned from the  $^{167}\text{Er}^{3+}$  transition.  $W(\omega, g_{\text{total}}, \Delta_{\text{ions}}, \omega_{\text{ions}})$  is the absorption rate of the cavity field by the ensemble of ions,  $W \sim \sum_i \frac{g_i^2}{\omega - \omega_i}$ , where  $g_i$  is the coupling between one ion and the cavity [5, 6]. We approximate the irregular inhomogeneous/hyperfine line as a Gaussian, and take from Reference [6] the expression for  $W$ :

$$W = i \frac{\sqrt{\pi \log 2} g_{\text{total}}^2}{\Delta_{\text{ions}}/2} \left[ 1 - \text{erfz} \left( -\frac{i\sqrt{\log 2}(\omega - \omega_{\text{ions}})}{\Delta_{\text{ions}}/2} \right) \right] \exp \left[ -\sqrt{\log 2} \left( \frac{\omega - \omega_{\text{ions}}}{\Delta_{\text{ions}}/2} \right)^2 \right], \quad (3)$$

where  $\Delta_{\text{ions}}$  is the linewidth of the ensemble transition,  $\omega_{\text{ions}}$  its the center,  $g_{\text{total}}^2 = \sum_i g_i^2$ . Finally, the ensemble cooperativity was computed using  $C = \frac{|W(\omega=\omega_{\text{ions}})|}{\kappa/2} = \frac{4\sqrt{\pi \log 2} g_{\text{total}}^2}{\kappa \Delta_{\text{ions}}}$  [7].

For the case with no initialization, the fit gave:  $\omega_{\text{cavity}} - \omega_{\text{ions}} = 2\pi \times 2.5$  GHz,  $g_{\text{total}} = 2\pi \times 0.79$  GHz,  $\Delta_{\text{ions}} = 2\pi \times 1.4$  GHz,  $C = 0.1$ .

For the case with initialization, the fit gave:  $\omega_{\text{cavity}} - \omega_{\text{ions}} = 2\pi \times 1.5$  GHz,  $g_{\text{total}} = 2\pi \times 0.70$  GHz,  $\Delta_{\text{ions}} = 2\pi \times 0.36$  GHz,  $C = 0.3$ .

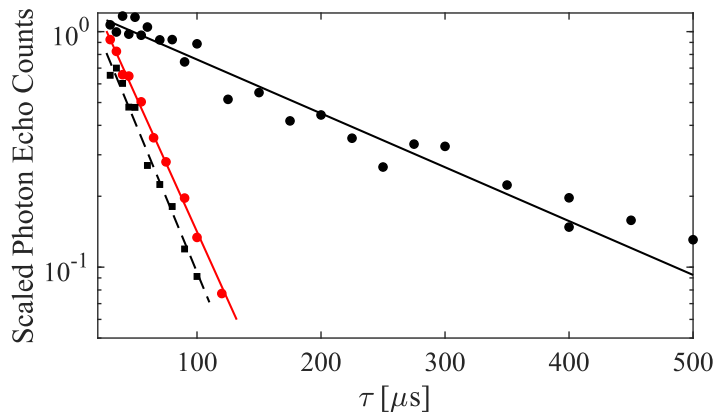
## V. COMPARISON OF THE OPTICAL $T_2$ TIME IN BULK AND IN THE NANOBEAM

By measuring two pulse photon echoes [8] as a function of time delay between pulses, the optical coherence time of ensembles of  $^{167}\text{Er}^{3+}$ :YSO ions was characterized in the center of the 1539 nm transition distribution, as shown in SM Figure 3. The laser was frequency stabilized by PDH locking to a home-built fiber cavity when measuring the bulk coherence at 35 mK ( $T_2 = 760 \mu\text{s}$ ). Without laser locking, this same curve had a double decay with a shorter exponential decay lifetime  $\sim 240 \mu\text{s}$ , which we interpret as being limited by laser frequency jitter. The coherence time of the ions coupled to the nanobeam cavity was  $\sim 1/4$  the coherence time of the bulk ions at the same temperature, but similar to the coherence time of the bulk ions at 1 K. It is likely that the measured coherence time of the ions coupled to the nanobeam is limited by heating due to the input pulse pairs, as the nanobeam has

poor thermal contact to the rest of the bulk crystal (through  $\sim 1 \mu\text{m}^2$  connections at either end). It was not possible to accurately simulate the device temperature during measurement due to lack of data on the low temperature thermal coefficient of YSO. It is also possible that the fabrication of the nanobeam resonator caused disorder that affected the coherence time of the ions. Rare-earth ions coupled to similar nanobeam resonators have been shown to have coherence times similar to the bulk [9, 10], however, the longer bulk coherence times measured in the current work allow a much more sensitive probe of the ions' environment.

## VI. ACCUMULATED VERSUS STEP-AND-PUMP ATOMIC FREQUENCY COMBS

Two different procedures were used to create the AFCs. For longer memory times, the frequency difference between the teeth of the comb must be smaller, so the teeth themselves need also be narrower. Laser frequency jitter limits the minimum width of comb teeth, so longer storage times necessitate frequency stabilization of the laser. With the step-and-pump method, the laser must be stepped in frequency, and the method used to lock the



SM Figure 3. Two pulse photon echo amplitudes versus inter-pulse time delay with exponential fits; the vertical axis is scaled for clarity.  $T_2$  was measured to be  $4 \times \tau(1/e) = 759 \mu\text{s} \pm 41 \mu\text{s}$  in bulk at 35 mK (black circles and solid black line fit),  $136 \mu\text{s} \pm 9 \mu\text{s}$  in bulk at 940 mK (black squares and dashed black line fit), and  $149 \mu\text{s} \pm 4 \mu\text{s}$  in the nanobeam at 42 mK (red circles and solid red line fit). All temperatures were measured at the dilution refrigerator stage to which the sample was thermally connected.

laser (feeding back to the current) did not allow for both stepping and stabilizing the laser frequency. With the accumulated AFC method, no frequency modulation is required, so frequency stabilization was possible, enabling longer memory times. However, for short memory times, where laser jitter did not adversely affect the width of the teeth, the step-and-pump method led to a higher efficiency because the depth of the teeth across the comb was homogeneous (with accumulated AFC, the frequency comb has a sinc function envelope).

## VII. FIDELITY MEASUREMENT

In the absence of a single photon source, a lower bound on the storage fidelity of a single photon input state can be found using the decoy state analysis method [11, 12]. In this method, a time bin state  $\psi$  with a mean photon number  $\bar{n}$  is stored using the AFC protocol, and the fidelity  $F_\psi^{(\bar{n})}$  of storage is measured as

$$F_\psi^{(\bar{n})} = \frac{N_\psi}{N_\psi + N_{\phi \perp \psi}}, \quad (4)$$

where  $N_i (i = \psi, \phi)$  is the number of photons measured in the output time bin corresponding to  $\psi$ , and  $\phi \perp \psi$  denotes the state orthogonal to  $\psi$ . The gain of the output,  $Q_\psi^{(\bar{n})}$  is also estimated using,

$$Q_\psi^{(\bar{n})} = N_\psi + N_{\phi \perp \psi}. \quad (5)$$

$F_\psi^{(\bar{n})}$  and  $Q_\psi^{(\bar{n})}$  are measured for mean photon numbers  $\bar{n}_1$  and  $\bar{n}_2$ , where  $\bar{n}_1 < \bar{n}_2$ , and  $\bar{n}_2 < 1$ . The lower bound on the fidelity of storing a one-photon input state  $F_\psi^{(n=1,L)}$  is then computed using:

$$F_\psi^{(n=1,L)} = 1 - \frac{E_\psi^{(\bar{n}_1)} Q^{(\bar{n}_1)} \exp \bar{n}_1 - E^{(n=0)} Y^{(n=0)}}{Y^{(n=1,L)} \bar{n}_1}, \quad (6)$$

where

$$E_\psi^{(\bar{n})} = 1 - F_\psi^{(\bar{n})} \quad (7)$$

is the error rate of storing a state  $\psi$  with mean photon number  $\bar{n}$ , and

$$Y^{(n=1,L)} = \max \left[ Y^{(n=0)}, \frac{\bar{n}_2}{\bar{n}_2 \bar{n}_1 - \bar{n}_1^2} \left( Q^{(\bar{n}_1)} \exp \bar{n}_1 - Q^{(\bar{n}_2)} \exp \bar{n}_2 \frac{\bar{n}_1^2}{\bar{n}_2^2} - \frac{\bar{n}_2^2 - \bar{n}_1^2}{\bar{n}_2^2} Y^{(n=0)} \right) \right] \quad (8)$$

is the lower bound on the detection yield for the storage of a single photon state (see Reference [11]).  $Y^{(n=0)} = Q^{(n=0)}$  is the yield when the input state is vacuum, equal to the dark counts in all output time bins. The superscripts denote photon number, and whether

the value is a lower bound ( $L$ ).  $E^{(n=0)}$  is the vacuum error rate, which is 0.5 by definition [11].

In order to obtain an average fidelity for all time bin states, the fidelities for storing time bin states  $|\text{early}\rangle$ ,  $|\text{late}\rangle$ ,  $|+\rangle = \frac{|\text{early}\rangle+|\text{late}\rangle}{\sqrt{2}}$  and  $|-\rangle = \frac{|\text{early}\rangle-|\text{late}\rangle}{\sqrt{2}}$  were measured for input photon numbers  $\bar{n} = 0.30$  and  $\bar{n} = 0.60$ . For input states  $|+\rangle$  and  $|-\rangle$ , an interferometer is required to measure  $N_\psi$  and  $N_{\phi\perp\psi}$ . Following Reference [13], a double atomic frequency comb was used as the interferometer, allowing for direct readout of  $F_+$  and  $F_-$ . The input pulses defining the  $|\text{early}\rangle$  and  $|\text{late}\rangle$  basis were 60 ns wide and 90 ns apart. A double AFC was used for measurements of all states, with the memory times associated with the two combs being  $t_1 = 210$  ns and  $t_2 = 300$  ns, such that  $t_1 - t_2 = 90$  ns. As SM Figure 4 shows, of the three output time bins, the first and third were used for measuring  $F_{\text{early}}$  and  $F_{\text{late}}$  while the second time bin was used for measuring  $F_+$  and  $F_-$ .

For computing the bound on the yield of a single photon in Equation 8,  $Q_-(Q_{\text{early}})$  and  $Q_+(Q_{\text{late}})$  were averaged to give  $Q_{+/-}$  ( $Q_{\text{early/late}}$ ), and the dark counts were averaged to give  $Y_{+/-}^{(n=0)}$  ( $Y_{\text{early/late}}^{(n=0)}$ ). From these, two different lower bounds on the single photon yield,  $Y_{+/-}^{(n=1,L)}$  and  $Y_{\text{early/late}}^{(n=1,L)}$  were computed. This was required because while the experiments to measure  $F_+$  and  $F_-$  were identical in every way except the input state, and the same holds for the experiments to measure  $F_{\text{early}}$  and  $F_{\text{late}}$ , the pairs of experiments differed from one another. For instance, because two output pulses overlapped to give a signal in measurements of  $F_+$  and  $F_-$ , the signal level was twice as large as for  $F_{\text{early}}$  and  $F_{\text{late}}$ , so the latter two experiments were conducted for twice as long to compensate.

Following Equation 6,  $F_+^{(n=1,L)}$  was therefore computed using:

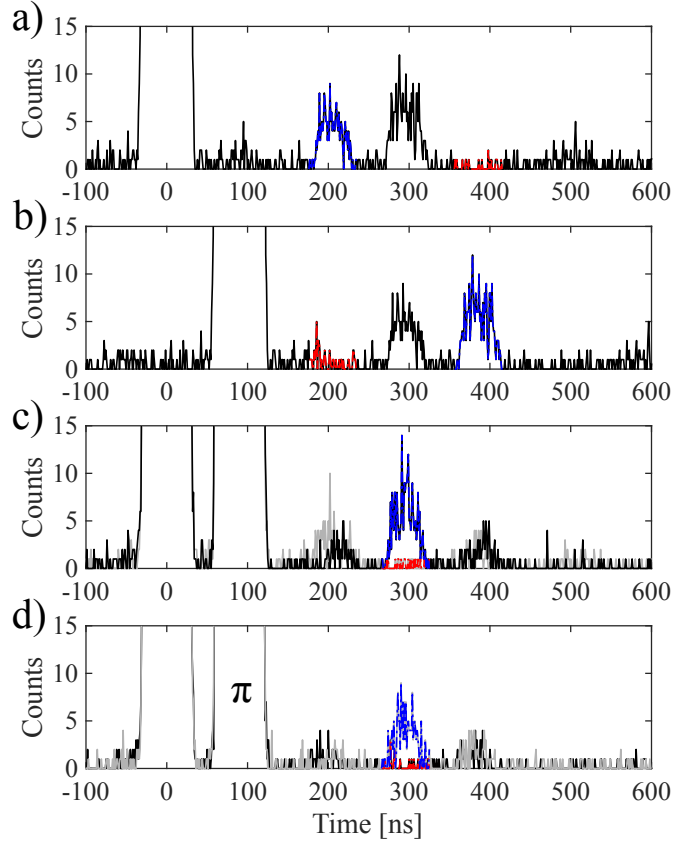
$$F_+^{(n=1,L)} = 1 - \frac{E_+^{(\bar{n}_1)} Q_{+/-}^{(\bar{n}_1)} \exp \bar{n}_1 - E^{(n=0)} Y_{+/-}^{(n=0)}}{Y_{+/-}^{(n=1,L)} \bar{n}_1}, \quad (9)$$

with similar equations for the other three states.

The lower bound on the fidelity of storing an arbitrary single photon state was then computed as follows:

$$F_{\text{average}}^{(n=1,L)} = \frac{1}{3} \left( \frac{F_{\text{early}}^{(n=1,L)} + F_{\text{late}}^{(n=1,L)}}{2} \right) + \frac{2}{3} \left( \frac{F_+^{(n=1,L)} + F_-^{(n=1,L)}}{2} \right). \quad (10)$$

Table I summarizes the fidelity data used to compute  $F_{\text{average}}^{(n=1,L)} = 93.7\% \pm 2.4\%$ . The



SM Figure 4. Part of the raw data used in the fidelity measurement.  $\bar{n} = 0.6$  input (left, cut off) and output pulses from double comb. Input pulses are time bin states a) early b) late, c) +, d) -. In all figures, blue (red) dash-dot line represents the 60 ns time bins counted as  $N_\psi$  ( $N_{\phi \perp \psi}$ ). Time resolution is 1 ns. The same data set, shown in a) and b), was used for both the early and late fidelity calculations, since absolute time is irrelevant. In this data set, a small pulse 100 ns after the read pulse can be seen. The origin of this pulse was unclear, but it disappeared in the absence of the double comb. In c) and d), the black curve represents data taken with comb detunings  $\delta_1 = \delta_2 = 0$ , while the grey curve represents data taken with  $\delta_1 = 0$ ,  $\delta_2 = \frac{\Delta_2}{2}$  ( $\phi_{\text{rel}} = \pi$ ).

uncertainties are calculated based on  $\sqrt{N_{\text{photon}}}$  standard deviation on all  $N_\psi$  values due to Poissonian statistics of photon counting and the uncertainty, estimated to be 15%, of the mean input photon numbers,  $\bar{n}$ .

There were two main limits to the measured fidelity. The first was dark counts, which are uniformly distributed SNSPD detection events with an average rate of 18 Hz, believed to be

Input photon number	$\frac{1}{2} (F_{\text{early}} + F_{\text{late}})$	$\frac{1}{2} (F_+ + F_-)$
$\bar{n} = 0.60 \pm 0.09$	$89.04\% \pm 1.34\%$	$91.90\% \pm 1.32\%$
$\bar{n} = 0.30 \pm 0.05$	$82.59\% \pm 1.80\%$	$90.75\% \pm 1.84\%$
$n = 0$	50%	50%
	$\frac{1}{2} (F_{\text{early}}^{(n=1,L)} + F_{\text{late}}^{(n=1,L)})$	$\frac{1}{2} (F_+^{(n=1,L)} + F_-^{(n=1,L)})$
$n = 1$	$89.85\% \pm 1.97\%$	$95.59\% \pm 3.37\%$

TABLE I. Measured fidelities of storage in the nanobeam device.

caused by environmental photons at a wide range of wavelengths and electronic noise. The dark counts limited fidelity bound was estimated to be  $\sim 96.5\%$ . The remaining reduction in measured fidelity was caused by the double AFC being an imperfect interferometer. Specifically, we observed: (i) imperfect cancellation of the overlapped output pulses in the case of destructive interference, resulting from the different efficiencies of output pulses generated by the two spectral combs; (ii) a peak found at  $\sim 100$  ns that is an unexpected result of the double comb procedure, shown in SM Fig. 4b.

### VIII. PREDICTED EFFICIENCY OF AFC STORAGE: CURRENT DEVICE AND FUTURE IMPROVEMENT

As described in References [5, 10, 14], the efficiency of an AFC memory in a resonator is given by:

$$\eta_{AFC} = \left( \frac{4\kappa_{\text{coupling}} \Gamma_{\text{comb}}}{(\kappa_{\text{total}} + \Gamma_{\text{comb}} + \Gamma_{\text{bg}})^2} \right)^2 \exp \left( -\frac{\pi^2}{2 \ln 2 (\Delta/\gamma)^2} \right). \quad (11)$$

The effective cooperativity  $C'$  of the atomic frequency comb is defined as:

$$C' \equiv \frac{\Gamma_{\text{comb}} + \Gamma_{\text{bg}}}{\kappa_{\text{total}}/2}, \quad (12)$$

where  $\Gamma_{\text{comb}}$  and  $\Gamma_{\text{bg}}$  are the absorption rates of the cavity field by the ensemble of ions in the comb and background, respectively. The background ions are the ions remaining after optical pumping, with transition frequencies where transparency is desired (i.e. between the teeth of the comb). Nonzero  $\Gamma_{\text{bg}}$  results from limitations in spectral holeburning, as discussed in Section II. Using  $\eta_{\text{spectral}}$ , the fractional optical depth of a spectral hole (in the language of Section II,  $\eta_{\text{spectral}} = d(t=0)$ ),  $\Delta$ , the inter-tooth spacing, and  $\gamma$ , the width of

one comb tooth, these can be estimated as follows:

$$\Gamma_{\text{comb}} \approx \eta_{\text{spectral}} \frac{\gamma}{\Delta} \Gamma_{\text{ions}}, \quad (13)$$

$$\Gamma_{\text{bg}} = (1 - \eta_{\text{spectral}}) \Gamma_{\text{ions}}, \quad (14)$$

where

$$\begin{aligned} \eta_{\text{spectral}} &= \frac{N_{\text{ions}}(\text{comb peak}) - N_{\text{ions}}(\text{comb trough})}{N_{\text{ions}}(\text{comb peak})} \\ &= \frac{\text{initial optical depth} - \text{optical depth post initialization}}{\text{initial optical depth}} \end{aligned}$$

and  $\Gamma_{\text{ions}} = |W(\omega = \omega_{\text{ions}})| = \frac{\sqrt{\pi \log 2} g_{\text{total}}^2}{\Delta_{\text{ions}}/2}$  is the absorption rate of the cavity field by the ensemble of ions before comb preparation (see Section IV). The effective cooperativity  $C'$  is therefore related to the cooperativity before the comb was created,  $C$  by  $C' = (\eta_{\text{spectral}} \frac{\gamma}{\Delta} + (1 - \eta_{\text{spectral}}))C$ . Rewriting the equation gives rise to the following expression for the memory efficiency of a real comb:

$$\eta_{\text{AFC}} = \left( \frac{1}{\frac{\Delta}{\gamma} \left( \frac{1}{\eta_{\text{spectral}}} - 1 \right) + 1} \frac{\kappa_{\text{coupling}}}{\kappa_{\text{total}}} \frac{4C'}{(1 + C')^2} \right)^2 \exp \left( -\frac{\pi^2}{2 \ln 2 (\Delta/\gamma)^2} \right). \quad (15)$$

The predicted efficiency for this device is  $\eta_{\text{AFC}} = 0.17\%$ , found using  $C = 0.3$ ,  $\frac{\kappa_{\text{coupling}}}{\kappa_{\text{total}}} = 0.21$ , a measured fidelity of  $\Delta/\gamma = 2.1$ , and by assuming a perfect comb  $\eta_{\text{spectral}} = 1$  (giving  $C' = 0.14$ ). This is similar to the measured value of  $0.20\%$  for a storage time of 165 ns.

To improve the memory efficiency, the two most important improvements that can be made are to increase the ensemble cooperativity, and to improve the ratio  $\frac{\kappa_{\text{coupling}}}{\kappa_{\text{total}}}$ . The first of these can be accomplished by increasing the doping of erbium in the YSO crystal ( $\times 4$  increase in  $C$  by increasing the ion concentration to 200 ppm, assuming no significant increase in inhomogeneous linewidth), and also by initializing into a single hyperfine state with 95% efficiency [4], before preparing a comb (an expected increase in  $C$  of approximately  $\times 2.5$ ). Using  $C = 3$  and  $\frac{\kappa_{\text{coupling}}}{\kappa_{\text{total}}} = 0.21$ , and a comb finesse of  $\Delta/\gamma = 3$ , ( $C' = 0.73$ ), the predicted efficiency is 3%.

At this point, the memory efficiency is mainly limited by the loss from the cavity. In the case of perfectly narrow, perfectly absorbing comb teeth with no background,  $C' \rightarrow 1$ ,  $\Delta/\gamma \rightarrow \infty$ ,  $\eta_{\text{spectral}} \rightarrow 1$ , the efficiency of the AFC becomes  $\left( \frac{\kappa_{\text{coupling}}}{\kappa_{\text{total}}} \right)^2 = \left( 1 - \frac{\kappa_{\text{intrinsic}} + \kappa_{\text{mirror 2}}}{\kappa_{\text{total}}} \right)^2$ . That is, in the limit of perfect spectral tailoring, the memory efficiency is limited by what fraction of the cavity decay rate is through the coupling port.

A memory efficiency greater than 90% can be achieved if the intrinsic quality factor of the resonator is increased from its current value of  $Q_i \sim 9000$  to 2 million, while increasing  $\frac{\kappa_{\text{coupling}}}{\kappa_{\text{total}}}$  to 0.97. The latter can be accomplished by making a resonator with one mirror having a relatively lower reflectivity, and with minimal losses through other channels (transmission through second mirror, scattering, absorption). This calculation assumes the same material as described above (200 ppm, ideal initialization into one hyperfine state), and a comb finesse of  $\sim 13$ . It also accounts for a decrease by a factor of  $\sim 3$  in the cooperativity that results from switching to a hybrid silicon-YSO platform where the cavity-ion coupling is decreased because the optical mode couples evanescently to the ions. At this efficiency, the memory would match the performance of an optical fiber (0.15 dB/km) at  $t_{\text{storage}} = 10 \mu\text{s}$  [15].

For a finesse of 13 and a storage time of  $10 \mu\text{s}$ , the corresponding comb tooth width is  $\gamma = \frac{\Delta}{\text{finesse}} = 8 \text{ kHz}$ . This is too narrow for a material doped with Kramer's ions such as  $^{167}\text{Er}^{3+}:\text{YSO}$ , where effective linewidths are limited by superhyperfine coupling to the host material's nuclear spins. In  $\text{Er}^{3+}:\text{YSO}$ , superhyperfine broadening is of the order of 1 MHz [16, 17]. However, long memory times can still be achieved with a nanoresonator in this material by using the spin-wave AFC, where the stored coherence is transferred from the optical to the hyperfine manifold and back [18]. Coherence times of greater than 1 second have been measured for the hyperfine levels in  $^{167}\text{Er}^{3+}:\text{YSO}$  [4].

- 
- [1] R. W. P. Drever, J. L. Hall, F. V. Kowalski, J. Hough, G. M. Ford, A. J. Munley, and H. Ward, *Appl. Phys. B* **31**, 97 (1983).
  - [2] T. Böttger, Y. Sun, C. W. Thiel, and R. L. Cone, *Phys. Rev. B* **74**, 075107 (2006).
  - [3] Y. Sun, T. Böttger, C. W. Thiel, and R. L. Cone, *Phys. Rev. B* **77**, 085124 (2008).
  - [4] M. Rančić, M. P. Hedges, R. L. Ahlefeldt, and M. J. Sellars, *Nature Physics* **14**, 50 (2018).
  - [5] M. Afzelius and C. Simon, *Phys. Rev. A* **82**, 022310 (2010).
  - [6] I. Diniz, S. Portolan, R. Ferreira, J. M. Gérard, P. Bertet, and A. Auffèves, *Phys. Rev. A* **84**, 063810 (2011).
  - [7] E. Miyazono, I. Craiciu, A. Arbabi, T. Zhong, and A. Faraon, *Opt. Express* **25**, 2863 (2017).
  - [8] I. D. Abella, N. A. Kurnit, and S. R. Hartmann, *Phys. Rev.* **141**, 391 (1966).
  - [9] T. Zhong, J. M. Kindem, E. Miyazono, and A. Faraon, *Nature Communications* **6**, 8206

- (2015).
- [10] T. Zhong, J. M. Kindem, J. G. Bartholomew, J. Rochman, I. Craiciu, E. Miyazono, M. Bettinelli, E. Cavalli, V. Verma, S. W. Nam, F. Marsili, M. D. Shaw, A. D. Beyer, and A. Faraon, *Science* (2017), 10.1126/science.aan5959.
  - [11] X. Ma, B. Qi, Y. Zhao, and H.-K. Lo, *Phys. Rev. A* **72**, 012326 (2005).
  - [12] N. Sinclair, E. Saglamyurek, H. Mallahzadeh, J. A. Slater, M. George, R. Ricken, M. P. Hedges, D. Oblak, C. Simon, W. Sohler, and W. Tittel, *Phys. Rev. Lett.* **113**, 053603 (2014).
  - [13] H. de Riedmatten, M. Afzelius, M. U. Staudt, C. Simon, and N. Gisin, *Nature* **456**, 773 (2008).
  - [14] S. A. Moiseev, S. N. Andrianov, and F. F. Gubaidullin, *Phys. Rev. A* **82**, 022311 (2010).
  - [15] Y.-W. Cho, G. T. Campbell, J. L. Everett, J. Bernu, D. B. Higginbottom, M. T. Cao, J. Geng, N. P. Robins, P. K. Lam, and B. C. Buchler, *Optica* **3**, 100 (2016).
  - [16] O. Guillot-Noël, H. Vezin, P. Goldner, F. Beaudoux, J. Vincent, J. Lejay, and I. Lorgeré, *Phys. Rev. B* **76**, 180408 (2007).
  - [17] B. Car, L. Veissier, A. Louchet-Chauvet, J.-L. Le Gouët, and T. Chanelière, *Phys. Rev. Lett.* **120**, 197401 (2018).
  - [18] M. Afzelius, C. Simon, H. de Riedmatten, and N. Gisin, *Phys. Rev. A* **79**, 052329 (2009).